Climate Risk Management 32 (2021) 100287

Contents lists available at ScienceDirect

Climate Risk Management

journal homepage: www.elsevier.com/locate/crm

Quantifying erosion hazards and economic damage to critical infrastructure in river catchments: Impact of a warming climate

Xiaorong Li [a,b,*], James R. Cooper [a], Andrew J. Plater [a]

[a] School of Environmental Sciences, University of Liverpool, Liverpool L69 7ZT, UK
[b] Energy and Environment Research Group, College of Engineering, Swansea University, Swansea SA2 8PP, UK

ARTICLE INFO

Keywords:
Erosion hazard
Economic impact
Climate change
River catchment
Decision making
UKCP18

ABSTRACT

Climate change is projected to cause considerable pressure on our environment and communities. In particular, an increase in flooding and extreme erosion events is foreseeable as a result of an anticipated increase in the frequency and severity of storms. In the absence of timely and strategic intervention, climate change is taking us closer to more uncertain (non-linear, stochastic) and potentially more catastrophic climatic impacts. This paper develops a state-of-the-art modelling framework to assess the economic impact of erosion hazards on critical infrastructure and evaluate their vulnerability and resilience to differing storm regimes. This framework is trialled on a UK town (Cockermouth, NW England) that has experienced significant storm-related erosion and flood damage in recent years, highlighting its ability to determine current and future erosion hazard to critical infrastructure. A hydro-sedimentary model is used to simulate fluvial and hillslope sediment erosion and deposition caused by extreme storms within river catchments (sheet, rill, gully and channel bank and bed erosion). The model is applied for current climate conditions and for two future epochs (2021–2040 & 2061–2080) to assess changing erosion hazard to critical infrastructure. Climate conditions for the two epochs are obtained using the UKCP18 high resolution realisation projections under emission scenario RCP8.5. The economic loss caused by these hazards is projected based on new, non-linear depth-cost curves derived from previous assessments. The results show that: 1) due to a warming climate, total rainfall in the Cockermouth area (and likely across the UK) may be higher for all storm durations and annual exceedance probabilities, until epoch 2061–2080 when the rainfall regime may shift towards shorter duration events with higher rainfall and longer duration events with less rainfall; 2) the total area that undergoes flooding, erosion and sediment deposition, and the magnitude of the hazard, may increase as the climate shifts; 3) the economic damage caused by erosion and deposition is positively related to rainfall total, and the highest costs are likely to be associated with damage caused to bridges (£102-130 million), followed by sediment deposition in the urban fabric (£9-82 million), and erosion damage to agricultural land (£16-26 million), buildings (£0.4-18 million) and roads (£0.4-4 million); and 4) the Estimated Annual Damage costs suggest that investment in bridges (£4-6 million) in the Cockermouth area is required now to ensure their resilience to extreme storm events, and interventions are likely to be needed within the next 20 years to prevent high economic costs associated with significant sediment deposition in the urban fabric (£0.3-4 million) and damage to roads (£0.08-0.1 million) and agricultural land (£0.6-2 million). This new framework can help support operational (immediate) and strategic (medium to

* Corresponding author.
E-mail address: xiaorongli.912@gmail.com (X. Li).

https://doi.org/10.1016/j.crm.2021.100287
Received 30 July 2020; Received in revised form 11 January 2021; Accepted 12 February 2021
Available online 19 February 2021

long term i.e. 10+ years) erosion control decision making through the provision of an assessment of the scale and consequences of erosion.

1. Introduction

Climate change is projected to cause considerable pressure on our environment and communities (Kellogg, 2019; Araújo & Rahbek, 2006). For certain parts of the world, climate change may lead to an increase in frequency and/or magnitude of precipitation (Palmer and Räisänen, 2002). For example, the UK Climate Projections 2018 (UKCP18) predict that average winter rainfall in the UK could increase by up to 35% by 2070. Further, Zappa et al. (2013) and Mizuta (2012) showed that the frequency and intensity of the most extreme storms, such as cyclones, will increase over the UK during the winter months (3% ± 5% increase in number and 3% ± 1% increase in intensity). This, in turn, will lead to increases in the frequency and magnitude of flood events as well as their associated damage and hazards (Milly et al., 2002).

Major advances have been made in the prediction of flood risk and the assessment of the vulnerability and resilience of critical infrastructure to river and surface flooding (e.g. Fewtrell et al., 2011; Yang et al., 2015; Coles et al., 2017). In the UK, the Environment Agency provides publicly available maps with predicted risk of flooding from rivers, sea and reservoirs (Environment Agency, 2013; DEFRA, 2016). Similarly, publicly available landslide hazard maps for vulnerable infrastructure and communities, such as those provided by the United States Geological Survey (USGS) in the USA, are available in many countries. Although numerous models exist for predicting river and slope erosion (e.g. Correa et al., 2016; Guan et al., 2016; Huang et al., 2016; Haregeweyn et al., 2017) and numerical studies have investigated impacts of land use and climate change on catchment-scale erosion and sediment yields (e.g. Boardman et al., 1990; Favis-Mortlock and Boardman, 1995; Howard et al., 2016), these have not resulted in an integrated computational framework with high capability to: (1) quantify the uncertainty in the risk posed by these hazards; (2) assess the impact of erosion hazards on critical infrastructure; (3) evaluate the physical and financial vulnerability and resilience of these assets to different storm regimes; or (4) communicate effectively these projections for decision support. Therefore, sustainable and resilient decision making for a changing climate is a challenge.

The impacts of erosion hazards in river catchments are, however, of strategic importance because they are wide ranging, costly and of critical importance to the vulnerability of assets (Thorne et al., 2007; Koks et al., 2019). For example, erosion can cause sedimentation in rivers, urban drainage structures and flood defences, incurring high maintenance costs and reducing the resilience of drainage networks to future flooding (e.g. Hoang & Fenner, 2016). In England and Wales, maintenance costs associated with urban drainage sedimentation are £50-60 M a year (Graves et al., 2015). Also, erosion causes considerable damage to key infrastructure such as bridges, roads, flood defences and dams (Deng and Wang, 2016; Li et al., 2019; Fluixá-Sanmartín et al., 2018), and contributes substantially to insurance claims (erosion accounts for 25% of valid subsidence insurance claims in the UK; Pritchard et al., 2013). Furthermore, erosion of farmland can cause considerable loss of soil and nutrients, reducing crop productivity or destroying crops directly (Morris & Brewin, 2014; Pierce & Lal, 2017). Finally, increased fine sediment loads in rivers due to erosion can be a primary

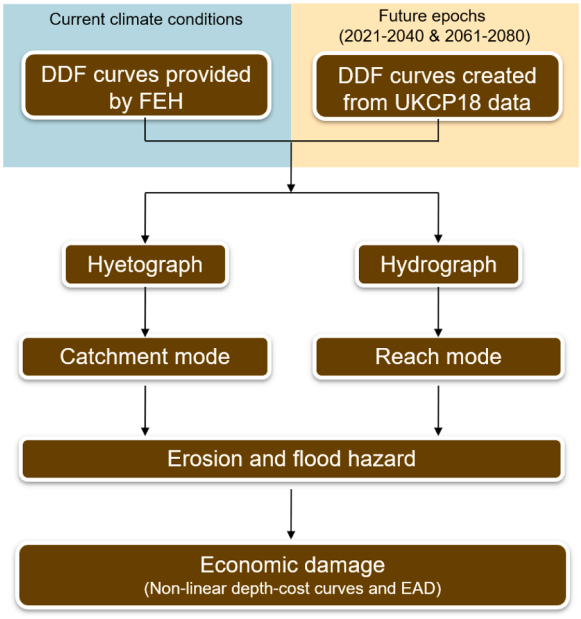

Fig. 1. Work flow of the erosion modelling framework. (DDF denotes Depth-Duration-Frequency, FEH denotes Flood Estimation Handbook, UKCP18 refers to the 2018 UK Climate Change Projections and EAD denotes Estimated Annual Damage).

carrier of chemicals posing a considerable source of water pollution, causing detrimental effects on ecosystem services, reducing water and habitat quality and increasing water treatment costs (Chatterton et al., 2010; Merz et al., 2010; Welter et al., 2010). Mobilisation of contaminants through soil erosion may be further exacerbated by wildfire events (Rothwell et al., 2007). In summary, storm-related erosion impacts are severe and far-reaching. Thus, establishing resilient, sustainable infrastructure depends on understanding the potential future risks of changing erosion hazards and their impact. In the absence of an integrated computational framework for assessing inland erosion risk we do not understand sufficiently: (i) the future risks posed to critical infrastructure; and (ii) how vulnerable and resilient these assets will be to increased frequency and severity of erosion hazards in a changing climate. Consequently, as identified by Prime et al. (2018), decision makers currently face questions about mitigation strategies that are very difficult to answer: (1) where to act to make an asset more resilient; and (2) when action is required: now or can investment be postponed?

This paper, therefore, aims to provide answers to these questions through the development of a state-of-the-art modelling framework and a suite of software tools that can be utilised for the probabilistic assessment, communication and mitigation of erosion risk. We trial this framework on a UK town (Cockermouth, NW England) that has experienced significant storm-related erosion and flood damage in recent years, highlighting its ability to determine current and future erosion hazard to critical infrastructure. A hydro-sedimentary model (CAESAR-Lisflood) is applied for current climate conditions and for two future epochs (2021–2040 & 2061–2080) to assess changing erosion hazard. The following scenarios for each epoch are explored, chosen to be consistent with UK national flood mapping (Environment Agency, 2013): (1) rainfall for three annual exceedance probabilities (3.3%, 1% and 0.1%); and (2) storm durations of 1, 3 and 6 h for each rainfall probability. Fig. 1 summarizes the workflow of this research. The creation of Depth-Duration-Frequency (DDF) curves, hyetographs and hydrographs is detailed in Section 2.

For a more holistic and integrated assessment of the scale and consequences of erosion, a set of methods, metrics, and tools are incorporated into the modelling framework to assess erosion impact potential beyond direct physical impacts. This approach is required because, with expected increased exposure of key assets to erosion, the potential for economic impacts cannot be ignored. Not only is it vital to evaluate and benchmark the conditions that lead to adverse erosion impacts and loss, it is equally important to provide a set of metrics to stakeholders for priority setting and decision making. To assess these hazards, flood maps, erosion depth maps, hazard maps and economic damage maps are created based upon the model results. To communicate the projections, the data are made available via a publicly accessible web-based decision support tool (DST, https://arcoes-dst.liverpool.ac.uk/EHRC/), that visualises and communicates erosion risk using decision-relevant terms and metrics. The DST mapping interface provides planning managers and the general public with a user-friendly means to visualize how storms with different annual exceedance probability and duration in current and future climatic conditions are predicted to cause increased flooding, erosion and economic loss to critical infrastructure. This research offers the first quantification of the risks posed by erosion hazards in an uncertain changing climate, and their economic impacts on critical infrastructure. In so doing, the paper highlights that erosion hazards have critical implications for the climate resilience of key rural and urban assets.

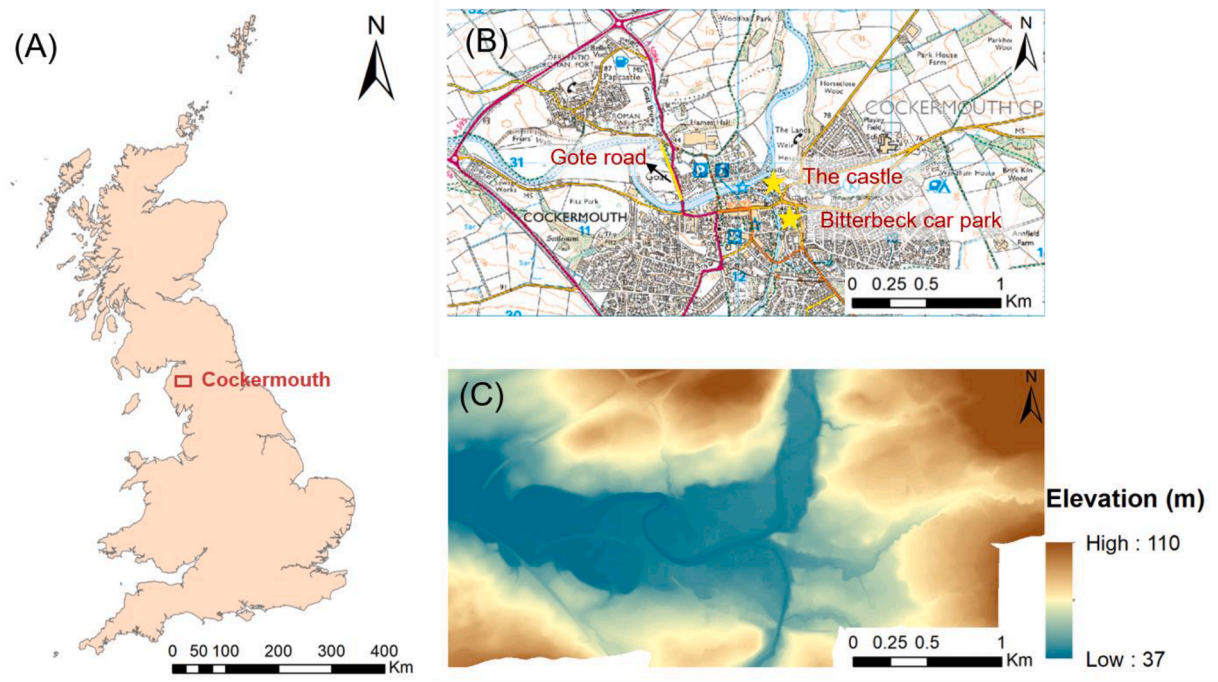

Fig. 2. (A) Geographic location of Cockermouth (created based on the UK Ordnance Survey GB National Outlines); (B) Ordnance Survey map of model domain (created based on the UK Ordnance Survey 1:25 000 Scale Colour Raster); (C) Topography of the model domain (created based on 1 m resolution LiDAR data – England Lidar Digital Terrain Model England (2009)).

2. Case study

The site selected to trial this methodology were the Cockermouth urban and rural areas in Cumbria, northwest England, UK (Fig. 2). This area was chosen for four reasons. First this area is historically prone to severe flooding and erosion damage from storm events, particularly in the last two decades, due to its geographic location. The town is situated outside the English Lake District on its northwest fringe. In general, the west of the UK receives more rain than the east because wet air from the Atlantic Ocean falls as rain as it travels over the western hills. Further, Cockermouth is at the confluence of two rivers (the River Cocker and the River Derwent) which conduit the runoff of two large catchments (catchments Derwent and Cocker with areas of 397.95 km^2 and 116.17 km^2) in the Lake District. Severe flood and erosion damage occurred most recently in 2005, 2009, and 2015. For example, the flood waters in 2009 inundated large parts of Cockermouth, severely damaging two road bridges and demolishing a key footbridge. Downstream in Workington, the floodwaters overwhelmed the Calva Bridge (A596) and destroyed the Northside road bridge (A597) and Navvies footbridge (Cumbria County Council, 2010). In the year 2015 alone, three major storms, storm Desmond (5–6 December 2015), Eva (24 December 2015), and Frank (29–30 December 2015), hit the town. Amongst the three storms, storm Desmond with an annual exceedance probability of 1.5–8% (95% confidence interval, Matthews et al., 2018) was the most extreme and had the largest impact on the town: more than 300 mm of rain fell over a 24-hour period and left 594 properties flooded (McCall & Evans, 2016). Secondly, in response to this event, the UK Environment Agency as a key Risk Management Authority, worked in partnership with Cumbria County Council as the Lead Local Flood Authority to release a Flood Investigation Report (McCall & Evans, 2016). This report records the progression of the storm event and the damage in detail, thus providing rare and extremely valuable validation data for the model framework. Thirdly, this area offers a strong test of the performance of the model, in so much as containing the confluence of two rivers, two catchments, urban and rural fabric, and a range of asset types. Finally, due to the severity of historical events and their occurrence, the climate change projections are of strong interest to stakeholders, including local governing authorities (e.g. Cumbria County Council), government agencies and departments (Department for Food & Rural Affairs, Environment Agency), emergency services (e.g. Cumbria First and Rescue Service), utility companies (e.g. National Grid, Electricity North West, United Utilities) and transport bodies (e.g. Highways England, bus companies).

3. Methods

3.1. The CAESAR-Lisflood model and hybrid catchment-reach approach

CAESAR-Lisflood is a two-dimensional cell-based hydro-sedimentary model combining the CAESAR landscape evolution model (Coulthard et al., 2013) for eroding and routing sediment, and the Lisflood-FP hydrodynamic model (Bates et al., 2010) for driving hillslope and fluvial runoff. This approach allowed sheet, rill, gully and channel bank and bed erosion to be simulated. This model was chosen as the modelling basis for the framework for two main reasons: (1) ability to resolve asset-scale hydraulics and erosion; and (2) ability to route sediment and water between the hillslope and fluvial system, and update topography at every time-step, thus allowing the impact of both hillslope and fluvial erosion to be explored (Coulthard & Skinner, 2016). In the model, the water flux (Q) between cells was calculated as follows:

$$Q = \frac{q - gh_{flow}\Delta t\frac{\Delta(h+z)}{\Delta x}}{(1 + gh_{flow}\Delta tn^2|q|/h_{flow}^{10/3})}\Delta x \tag{1}$$

where q is the water flux per unit width from the previous iteration [m^2s^{-1}]; g is acceleration due to gravity [ms^{-2}]; h is water depth [m]; z is bed elevation [m]; h_{flow} is the maximum depth of flow between cells [m]; n is Manning's coefficient [$s\ m^{-1/3}$]; Δx is the grid cell width [m]; and Δt is the time step [s].

Flow depth and velocity within a cell was calculated from this flux using the Manning's (1890) equation:

$$Q = uA = \frac{1}{n}h^{2/3}AS^{0.5} \tag{2}$$

where h is cell flow depth [m]; u is cell flow velocity [$m\ s^{-1}$]; S is the cell slope [–]; n is Manning's coefficient [$s\ m^{-1/3}$]; and A is the cross-sectional area of the cell ($A = hx$) [m^2].

Bed shear stress (τ) was calculated based on the cell flow velocity:

$$\tau = \rho C_d u^2 \tag{3}$$

where ρ is density of water [$kg\ m^{-2}$] and C_d is a drag coefficient [–] determined using:

$$C_d = gn^2h^{0.33} \tag{4}$$

Bed shear stress in each cell was then compared with the critical shear stress of sediment in that cell to determine the erosion/deposition conditions in the domain. This was carried out using either the Einstein (1950) or Wilcock and Crowe (2003) sediment transport formulae. The erosion and deposition depths (E/D depths) were then used to calculate the topography change caused by water flow in each iteration. CAESAR-Lisflood allows up to nine sediment grain-size classes to be defined in the model, and this grainsize variability is expressed both vertically and horizontally. Please refer to Van De Wiel et al. (2007) for a detailed description of

the model controlling equations, including the formula in Wilcock and Crowe (2003), used in this paper because of its ability to predict fine and coarse fractions within sediment mixtures.

CAESAR-Lisflood has two simulation modes: catchment mode and reach mode. In catchment mode, rainfall is cast across the catchment area evenly to generate runoff using an adaptation of the rainfall-runoff model TOPMODEL (Beven and Kirkby, 1979; Welsh et al., 2009). The resulting runoff is then routed to determine overland flow depth, flow velocity and hillslope erosion according to the methods described above. The model is driven in part by the soil hydraulic conductivity which is represented by a parameter *m*. This parameter *m* controls the effective depth or active storage of the catchment soil profile. Essentially, the *m* value affects the proportion of rainfall that reaches the river channel by overland flow; an increase in *m* reduces the transmissivity within the soil and thus reduces the discharge within the river channel (Beven and Kirkby, 1979; Beven, 2011). In reach mode, a known water discharge is inputted directly at the upstream end of a river reach of interest, and subsequently routed within-channel and on the floodplain during flood conditions. The resulting hydraulics are used to estimate fluvial erosion in each cell. To assess erosion hazards in the river catchment, therefore, a hybrid approach was adopted to combine the advantages of both modes; the capability of the catchment mode to simulate hillslope runoff and erosion and to route water and sediment fluxes to the fluvial system, and the capability of the reach mode to simulate river flooding and erosion. In this hybrid approach, the model was run twice, once in catchment mode and once again in reach mode. The results of the two modes were then combined to estimate maps of erosion and deposition depth. Sediment depth, rather than rates or mass, are presented because the depth of sediment is most critical when assessing impacts on assets, such as the damage to roads, bridges, buildings and utilities.

3.2. *Creation of hyetographs and hydrographs*

To drive the hybrid model, hyetographs and hydrographs were required as input for the catchment mode and reach mode respectively. These were created from rainfall DDF curves following the Revitalised Flood Studies Report/Flood Estimation Handbook (FSR/FEH) rainfall-runoff method developed for UK catchments (Kjeldsen et al., 2005). A detailed explanation of this method is provided in the Supplementary Material (Text S1). These curves describe rainfall depth as a function of duration for a given annual exceedance probability. Hence a curve defines the rainfall depth of a storm event that is expected to occur at a location for a given probability of occurrence and a given duration. For current climate conditions, DDF curves for catchments Derwent and Cocker were obtained from the UK Flood Estimation Handbook web service (https://fehweb.ceh.ac.uk/). For future climate conditions, DDF curves were constructed, following the method described in Overeem et al. (2008), using data from the UKCP18 high resolution realisation (2.2 × 2.2 km cell) projections. To do this, hourly rainfall data for the two catchments was downloaded from dataset 'UKCP18 Local Projections at 2.2 km resolution for 1980-2080′ (http://data.ceda.ac.uk/badc/ukcp18/data/land-cpm/uk/2.2km), based on the RCP8.5 emission scenario. This dataset is the only one available from the 2018 UK Climate Change Projections (UKCP18) that provides hourly rainfall data, chosen so that high impact events such as short, intense localised storm events can be simulated. The two future epochs (2021–2040 & 2061–2080) and emission scenario were dictated by this dataset. The dataset contains hourly rainfall derived from 12 projections from the HadREM3-RA11M model, each driven by the 12 perturbed variants of the HadREM3-GA705 model (Lowe et al., 2018). The scope of this paper is to demonstrate the broad feasibility and the capability of the modelling framework, and thus one of these 12 projections was used. From the hourly rainfall data, annual maxima were identified for each epoch, each rainfall event duration (1 h, 3 h & 6 h) and each grid point within the catchments. These annual maxima were then concatenated to form station-year records to which generalized extreme value (GEV) distributions were fitted to produce an estimate of total rainfall for the selected annual exceedance probabilities (3.3%, 1% & 0.1%). This total rainfall was then symmetrically distributed over the event duration, with the peak rainfall assumed to occur in the middle of the storm. The detailed steps are described in the Supplementary Material (Text S2). Fig. 3 shows an example of a hyetograph and hydrographs produced following the method above. The examples are for a 3-hour storm during epoch 2021–2040 with an annual exceedance probability of 1%.

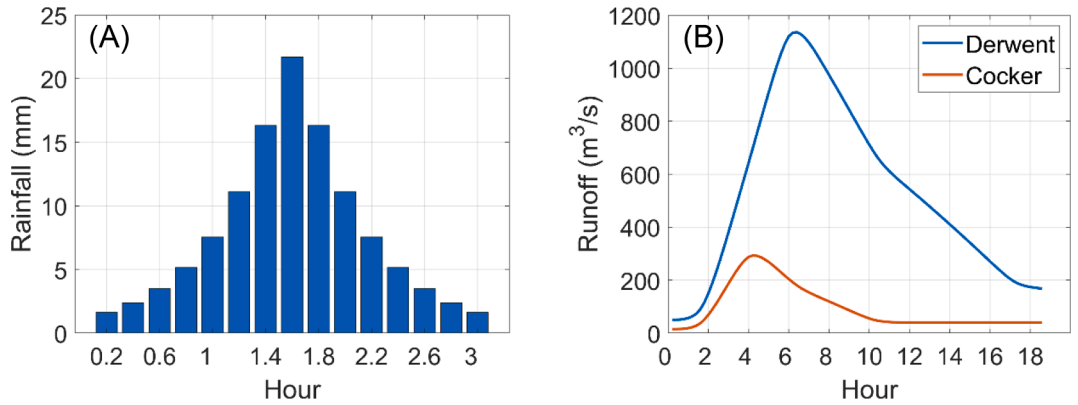

Fig. 3. (A) Hyetograph and (B) hydrographs for a 3-hour storm during epoch 2021–2040 with an annual exceedance probability of 1%.

3.3. Economic assessment of potential damage from erosion hazards

To quantify the impact of erosion hazards, and the vulnerability of assets, the focus was on economic loss. This approach was taken because these hazards rarely pose a direct risk to human health in the UK (noting that some regions in the world may not be as fortunate), and decisions on whether to intervene to control erosion involve judging the cost of the proposed measure against the associated economic benefits i.e. the economic damages that would be reduced by the associated spending (Lane et al., 2011). To estimate the damage averted if erosion control was present and therefore estimate the "revenue" generated by investing in intervention, Estimated Annual Damage (EAD) for each land-use type and for each epoch was calculated according to Equation (5). The desire was to assess the broad feasibility of the framework so the paper examines a range of asset types; the economic loss caused by erosion to buildings, roads, bridges and land, and sediment deposition on the urban fabric.

$$EAD = sum\left(\frac{Cost_{1hr}^{prob} + Cost_{3hr}^{prob} + Cost_{6hr}^{prob}}{3} \times prob\right),\ prob = 3.3\%, 1\%\&0.1\% \tag{5}$$

Estimates of economic loss (*Cost*) on an event basis for each model cell were produced based upon fixed costs or unit costs. These costs are related to the severity of damage in terms of erosion and deposition depth for each type of land use and infrastructure for the modelled events. The UK Ordnance Survey MasterMap (Topography Layer) was overlaid with the model domain in GIS to determine the land-use type of each model cell. Fixed costs and unit costs are detailed in Tables 1A–1E. Some of the costs were described by depth-cost curves (e.g. costs for buildings for erosion depth of 1–3 m) similar to the types of curves used for assessing flood costs (e.g. Penning-Rowsell et al., 2014).

4. Model setup

Fig. 2 shows the domain of the model, which has a mesh resolution of 2 m. This resolution was chosen to ensure that land-use features, such as houses, bridges and roads, were resolved in the model, balanced with the desire to simulate the entire town and its surroundings hillslopes. To construct the topography, Environment Agency 1 m resolution airborne laser altimetry (LiDAR) data was interpolated onto the grid. Before running the above-mentioned scenarios, the model was applied to re-create the 2015 storm Desmond for model validation. In this case, the model was run twice following the hybrid approach, once in catchment mode and once again in reach mode. The catchment mode was driven using hourly rainfall (Fig. 4A) measured at Honister Pass (location see Fig. 4C) during storm Desmond.

The soil hydraulic conductivity m within the rainfall-runoff model was calibrated by minimising the difference between the observed and simulated runoff in the Derwent. This calibration gave a m value of 0.005 m. The observed runoff data was taken from hourly river discharge records at the Environment Agency gauging station at Ouse Bridge (Fig. 4B). The reach mode was driven by hourly river discharge records at Ouse Bridge and the Southwaite Bridge gauging stations on the Derwent and Cocker (Fig. 4C), respectively. A fixed Manning's number of 0.04 s $m^{-1/3}$ was chosen to represent most closely the channel conditions found in the two rivers (channel type 2a: mountain streams with little in-channel vegetation, steep banks and predominantly gravel and cobble beds; Chow, 1959). A detailed description of the model parameters and their values are given in Table S7.

The domain was segregated into three categories: urban areas, hillslopes and river channels. The latter two categories have distinctly different sediment compositions. These compositions were derived from the British Geological Survey (BGS) soil texture map (http://mapapps2.bgs.ac.uk/ukso/home.html). The soil on the hillslopes is composed of clay, loam, silt and sand, and sediment in the river channels is mainly gravel and cobble. Without sufficient information on the spatial variation in these compositions, they were set as spatially invariant within the respective hillslope and fluvial systems. Structures (e.g. buildings) in urban areas were set as immobile, roads were set with a critical shear stress for tarmac (Dong et al., 2017), and parks and fields in urban areas were treated the same as hillslopes. Further details on sediment classification and composition can be found in the Supplementary Material (Table S8).

Table 1A
Depth – cost values for buildings; x is erosion depth, y is cost.

Erosion depth (m)	Cost (£)	Description
0–0.5	926.00 (Home Advisor, 2019)	Cost of soil replenishment and consultation per house
0.5 – 1	3,716.00 (Home Guide, 2019)	Cost of foundation repair and clean up per house
1 – 3	$y = 16917x^2 - 12750x + 903$ (Constructed based on the costs for 0–0.5 and 0.5–1 m above and de Castella, 2011)	Cost to repair
greater than 3	1990*Area (Costmodelling Limited, 2020)	Cost of a new build

(See Supplementary Material Text S3 for detailed description).

Table 1B
Depth – cost values for roads; x is erosion depth, y is cost.

Erosion depth (m)	Cost (£)	Description
<0.1	0.00	No cost
>0.1	100*Area	Cost of repairing embankments of A roads

(Source: Hertfordshire County Council (2020))

Table 1C
Depth – cost values for bridges; x is erosion depth, y is cost.

Erosion depth (m)	Cost (£)	Description
0–0.5	38.00 (McGowan, 2016)	Cost to inspect per m^2
0.5 – 3	$y = 8366^2 + 61789x - 9691$ (Constructed based on McGowan, 2016)	Cost to repair
>3	250,000.00 (McGowan, 2016)	Cost to install a temporary bridge

(See Supplementary Material Text S3 for detailed description).

Table 1D
Depth – cost values for agricultural land; x is erosion depth, y is cost.

Erosion depth (m)	Cost (£)	Description
Any	20.50 (Rickson et al., 2010)	Cost per tonne

(See Supplementary Material Text S3 for detailed description).

Table 1E
Depth – cost values for urban fabric; x is deposition depth, y is cost.

Deposition depth (m)	Cost (£)	Description
0 – 0.2	200.00	Cost of road clearance per m^2
>0.2	$y = 1001x^2 - 100x$(Constructed based on the cost for 0–0.2 m above and My Job Quote, 2019)	Cost of clearance and drainage unblocking per m^2

(Urban fabric includes roads, tracks and paths. When deposition depth is less than 0.5 m, an assumption is made that only clearance of deposited sediment from the surface of the above-mentioned assets is required. When deposition depth is greater than 0.5 m, the assumption is that the amount of sediment that falls into the urban drainage system has surpassed its carrying capacity and unblocking is required. See Supplementary Material Text S3 for a detailed description.)

5. Results

5.1. Model validation

Fig. 5 shows the simulated extent of flooding and the extent of flooding recorded in the Flood Investigation Report (McCall & Evans, 2016). The good agreement between the two flooding extents demonstrates the strong capability of CAESAR-Lisflood to simulate the extent of the 2015 flood event. Fig. 6 shows the simulated erosion/deposition depths in which the topographic changes in small tributaries are the result of the erosion simulated in catchment mode. Three severely eroded areas documented in the report, the riverbank at the castle, Bitterbeck car park and east of Gote Road, are captured by the model, showing that the model is able to provide reliable spatial estimates of erosion.

To assess the reliability of the model in producing erosion and deposition depths quantitatively, histograms of model-predicted and LiDAR-derived erosion and deposition depths are compared in Fig. 7. LiDAR datasets were available from only 2009 and 2017 to represent land elevations before and after storm Desmond. LiDAR data suggests that much of the topographic change ranged between −1 and 1 m (99.5% of the pixels). The model also predicts the vast majority of erosion and deposition occurs within the range of −1 to 1 m (92.7% of the pixels), which reflects well the estimates from the LiDAR data. However, the model predicts more drastic changes, such as erosion of up to 4 m. This scale of erosion was documented along the riverbanks in the Flood Investigation Report (McCall & Evans, 2016), such as at the castle, but not seen in the LiDAR data. We believe this disparity occurs because of the temporal offset of the LiDAR data. The LiDAR data used to represent conditions after the storm was collected nearly 2 years after the actual occurrence of storm Desmond; the large depths of deposition were likely cleared from the urban fabric, and the severe erosion along the riverbank was repaired (e.g. Photograph 1 in the Flood Investigation Report by McCall & Evans, 2016). Nonetheless, the possibility the model overestimates elevation changes, and subsequently the economic damages, cannot be totally discounted.

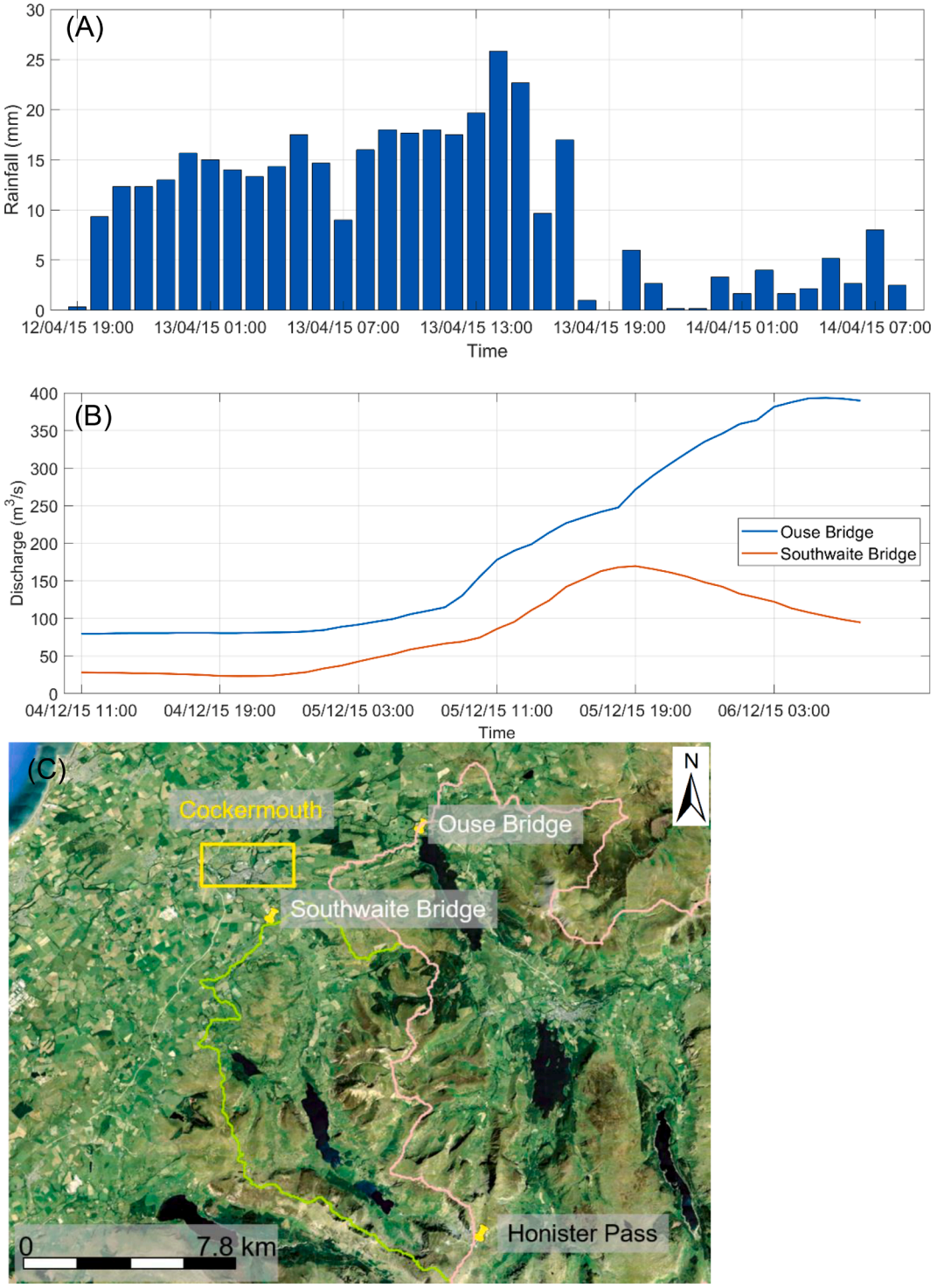

Fig. 4. (A) Hourly rainfall measured at Honister Pass during storm Desmond; (B) Hourly river discharge records at Ouse Bridge and the Southwaite Bridge gauging stations on the River Derwent and Cocker; (C) Gauging station locations (created based on Google Earth imagery). The pink line denotes the boundary of the Derwent catchment and the green line the boundary of the Cocker catchment. (For interpretation of the references to colour in this figure legend, the reader is referred to the web version of this article.)

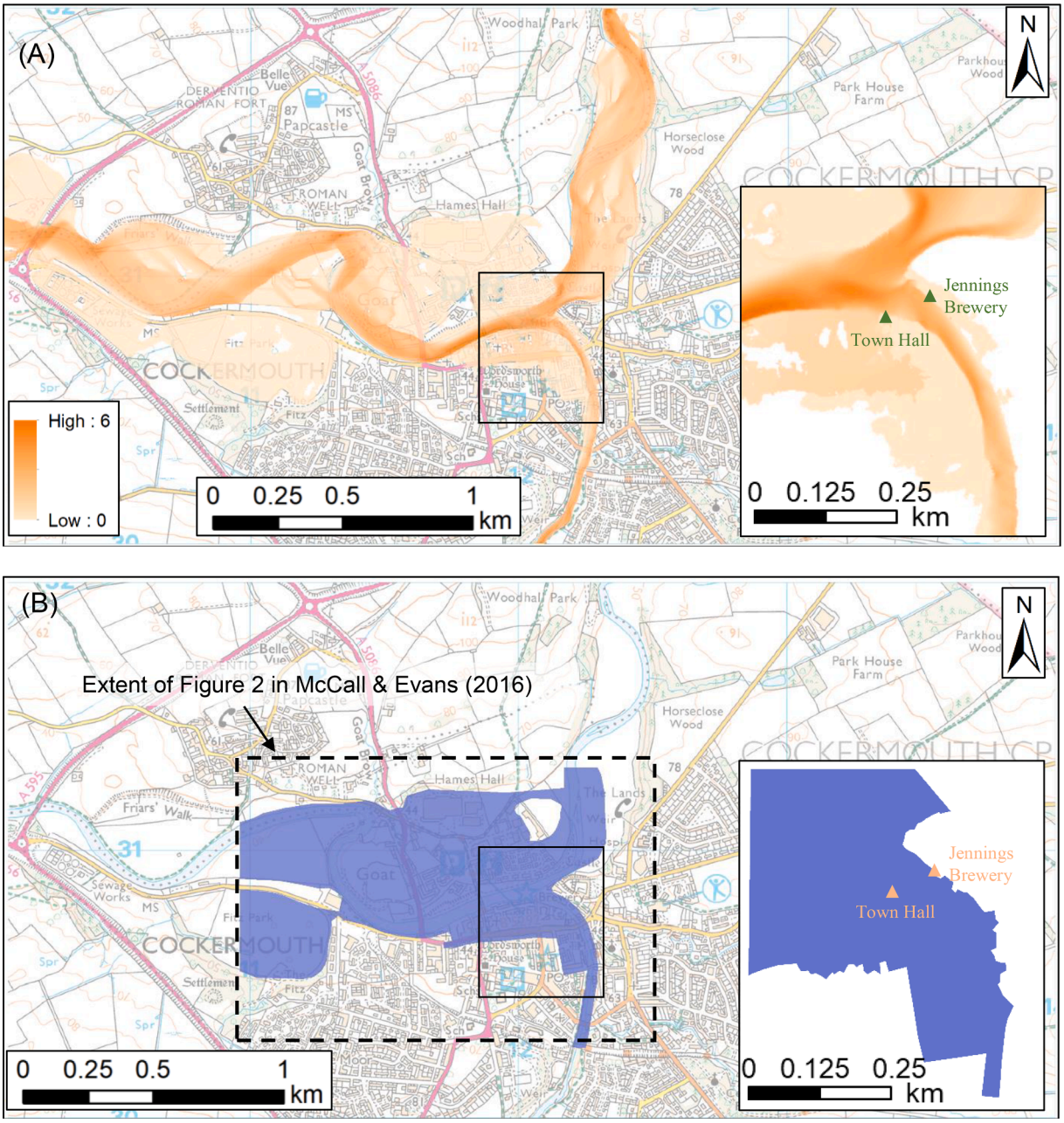

Fig. 5. (A) Simulated extent of flooding for storm Desmond. The colours indicate water depth; (B) Extent of flooding based upon Fig. 2 in McCall & Evans (2016) for storm Desmond. Solid insets show extent of flooding along the bank of the River Cocker. This area includes a mix of retail and residential properties, as well as Jennings Brewery and Cockermouth Town Hall.

5.2. Storm rainfall totals

Fig. 8 shows the estimated total rainfall for the three annual exceedance probabilities (3.3%, 1% and 0.1%). Total rainfall values for the future two epochs are calculated using the DDF curves. Compared with the baseline (current conditions), rainfall totals for the two future epochs increase, reflecting a warming climate. For the baseline and epoch 2021–2040, rainfall totals increase as storm duration lengthens. For epoch 2061–2080, however, the rainfall totals show the climate is moving towards shorter duration events with higher rainfall and longer duration events with less rainfall. In particular, rainfall totals for 6-hour storms are smaller than those for 3-hour storms. The percentage increase in total rainfall compared with the baseline increases with duration, except for 6-hour storms in epoch 2061–2080, and rises with annual exceedance probability. Since these rainfall totals are derived from one climate scenario from the UKCP18 2.2 km local projections, the rainfall changes between epoch 2021–2040 and epoch 2061–2080 could include both inherent

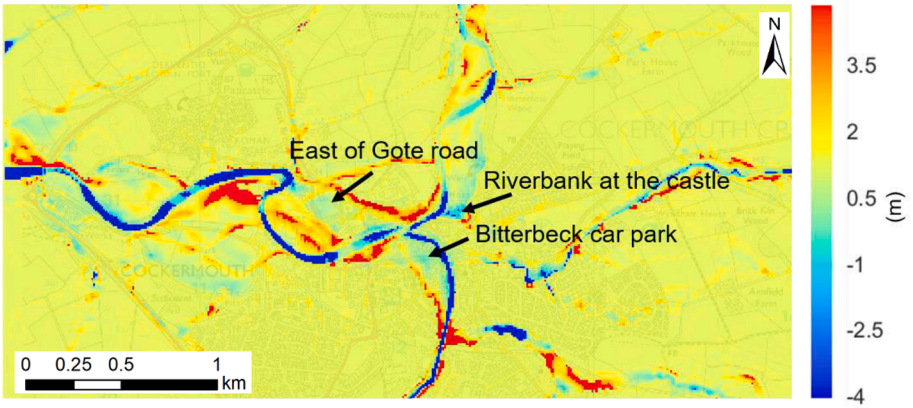

Fig. 6. Predicted erosion and deposition depths for storm Desmond. The scale shows changes in elevation (positive values indicate deposition while negative values indicate erosion).

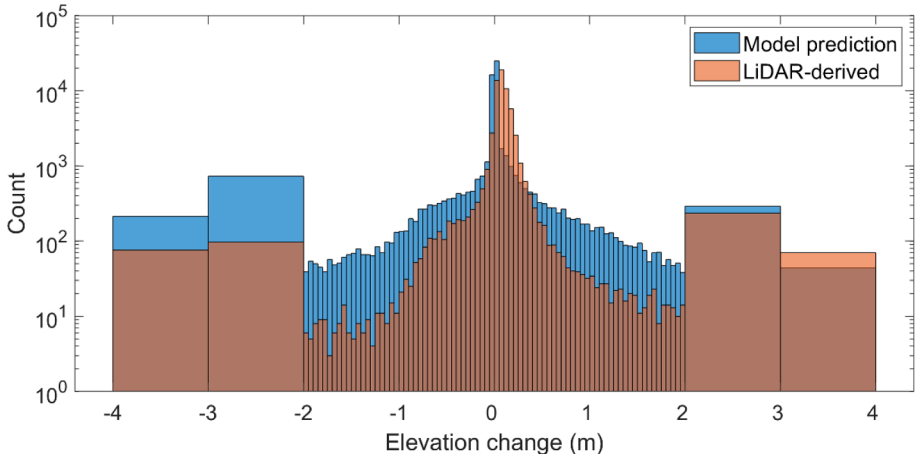

Fig. 7. Histograms of erosion and deposition depths produced by the model and those derived from LiDAR data collected in year 2009 and year 2017, for storm Desmond. Note that the dark brown shading is a result of light brown (LiDAR-derived) overlaying blue (Model prediction). (For interpretation of the references to colour in this figure legend, the reader is referred to the web version of this article.)

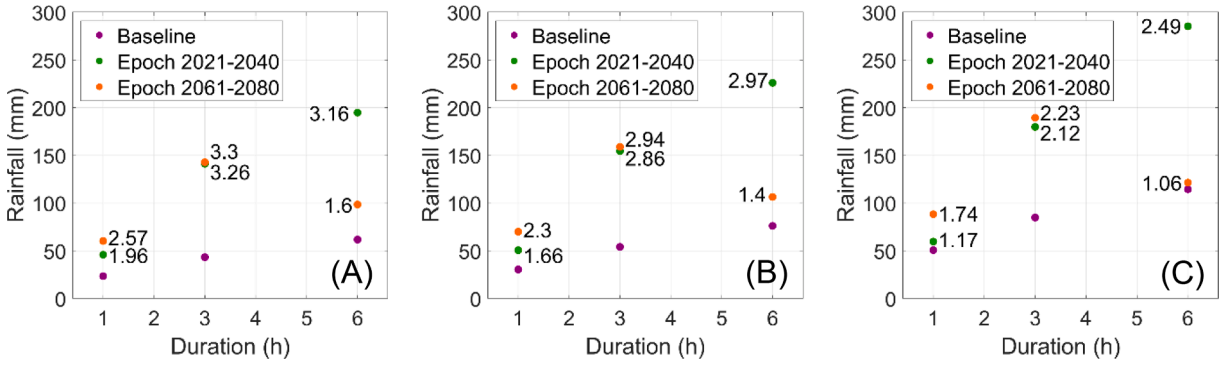

Fig. 8. Total estimated rainfall for the three annual exceedance probabilities: (A) 3.3%; (B) 1%; and (C) 0.1%. Numbers in the figures are ratios between rainfall of each future epoch and the current climate conditions (Baseline).

variability and long-term climate regime shift.

5.3. Extent of flooding

Fig. 9 shows the extent of flooding for the worst case scenario – a 6-hour storm with an annual exceedance probability of 0.1% during epoch 2021–2040. Results for the other scenarios are displayed in the Supplementary Material (Fig. S5–7) and on the web-based DST. In this case, a large portion of the urban area on the north side of the River Derwent is flooded. The banks of the River Cocker, the commercial area on the west side of the Cocker, and the grounds of the Jennings Brewery at the confluence where the two rivers meet are also flooded. Severe flooding in both the upstream and downstream areas of the River Derwent is also observed. Although these areas are mainly fields, they support a number of community assets, such as the Cockermouth Cricket Club on the west side of Gote Road and Fitz Park on the west end of the town, which are frequently visited for recreational activities. More significantly, the sewage works on the west edge of the town are also flooded.

The total estimated flooded areas for all the scenarios are shown in Fig. 10. The corresponding hazard rating, calculated according to Table 3.2 in HR Wallingford (2006) is presented in the Supplementary Material (Fig. S8–10). Given the severity of the storm event, the hazard rating of the flooded areas is mostly either 'Significant' (16.5% of the total flooded area) or 'Extreme' (20.5% of the total flooded area), i.e. owing to the deep fast flowing water, the flood zones are hazardous to life. The numbers in Fig. 10 are the ratios of total flooded area compared with the baseline. The trend with climatic conditions is similar to that of rainfall totals: the total flooded area increases for the two future epochs. The area also increases as the annual exceedance probability becomes higher. The areas being flooded for the 6-hour storms in epoch 2061–2080 are smaller than those in epoch 2021–2040. Owing to the shift of the climate towards shorter duration rainfall events with higher rainfall, the flooded area is also smaller than those for 3-hour storms in the same epoch.

A warming climate significantly increases the flood extent. For example, for the 3-hour duration events, storms with an annual exceedance probability of 3.3%, 1% and 0.1% during epochs 2021–2040 and 2061–2080 flood an additional 0.73, 0.67, 0.52 and 0.75, 0.71, 0.57 km^2 of land, respectively. These extents predominantly include the urban areas north of the River Derwent, the commercial area on the west side of the River Cocker, Fitz Park and the sewage works on the west edge of the town (for details please visit Fig. S5–7 in the Supplementraty Material and the web-based DST). Viewed from a perspective of percentages (Fig. 11), the warming climate represents substantial increases in inundation for short duration events with higher annual exceedance probability, whereas, for short duration events with lower annual exceedance probability, the percentage increase is smaller because a large area is already flooded by extreme storm events with a lower probability of occurrence. For example, moving from the baseline to epoch 2021–2040, flood extent increases more than 8-fold for a 1-hour storm event with an annual exceedance probability of 3.3%, but by 62% for a 1-hour storm event with an annual exceedance probability of 0.1%. Also, moving from the baseline to epoch 2061–2080, flood extent increases more than 10-fold for a 1-hour storm event with an annual exceedance probability of 3.3%, but by 136% for a 1-hour storm event with an annual exceedance probability of 0.1%. As the duration of the event increases, the effect of annual exceedance, however, becomes smaller. For example, for the 3-hour storm events in epoch 2021–2040, the flooded area increases by between 108% and 317% (a difference of 209%) from the baseline conditions. When the duration increases to 6 h, this increase is between 178% and 251%, a difference of just 73%. Further, the impact of duration diminishes as the annual exceedance probability becomes lower. For example, for events with an annual exceedance probability of 3.3% in epoch 2021–2040, the flooded area caused by storms with different durations varies from 199% to 795%, whereas, for events with an annual exceedance probability of 0.1% in the same epoch, the area only varies from 62% to 178%.

5.4. Flood depth and velocity

Fig. 12 shows the probability density functions of water depth for all the scenarios. Numbers in the plots are the corresponding means and standard deviations (in brackets) of water depths. Over time (from baseline to epoch 2061–2080) the mean depth decreases

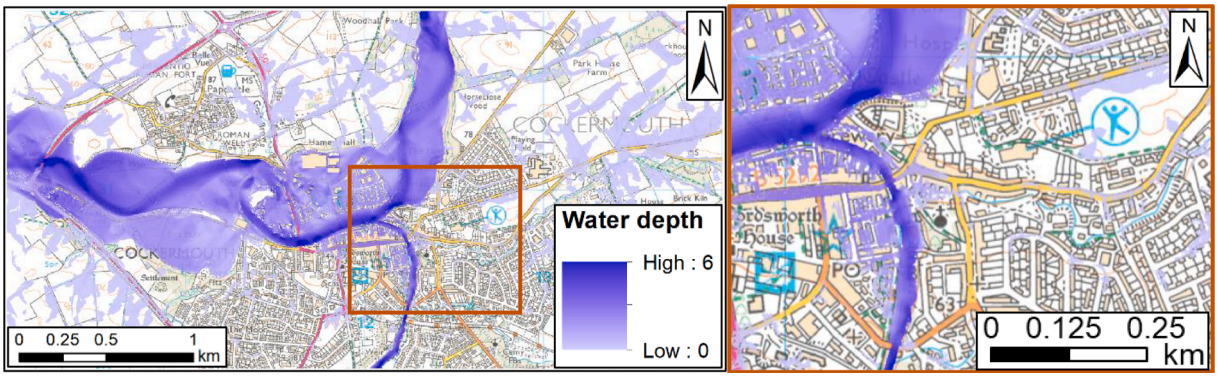

Fig. 9. Flood depths (m) for the worst case scenario – a 6-hour storm with an annual exceedance probability of 0.1% during epoch 2021–2040.

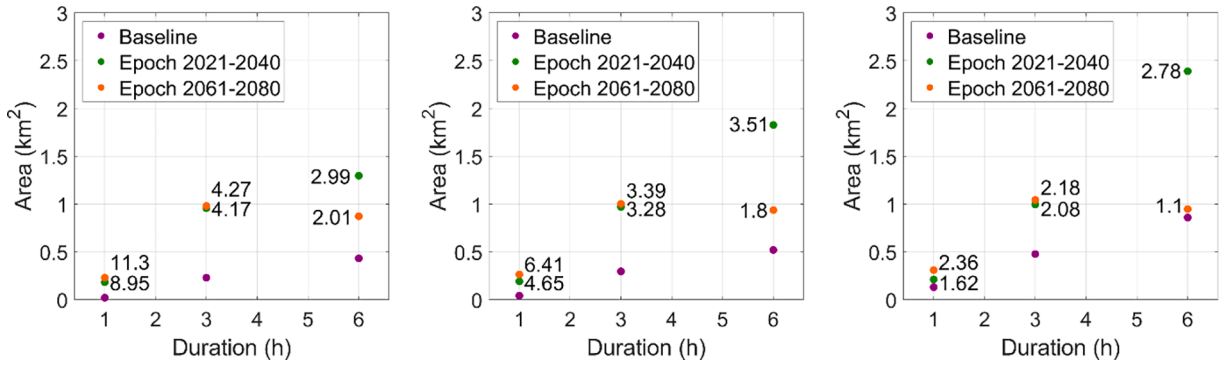

Fig. 10. Total area flooded for the three annual exceedance probabilities: (A) 3.3%; (B) 1%; and (C) 0.1%. Numbers in the figures are ratios between total flooded area of each future epoch and the current climate conditions (Baseline).

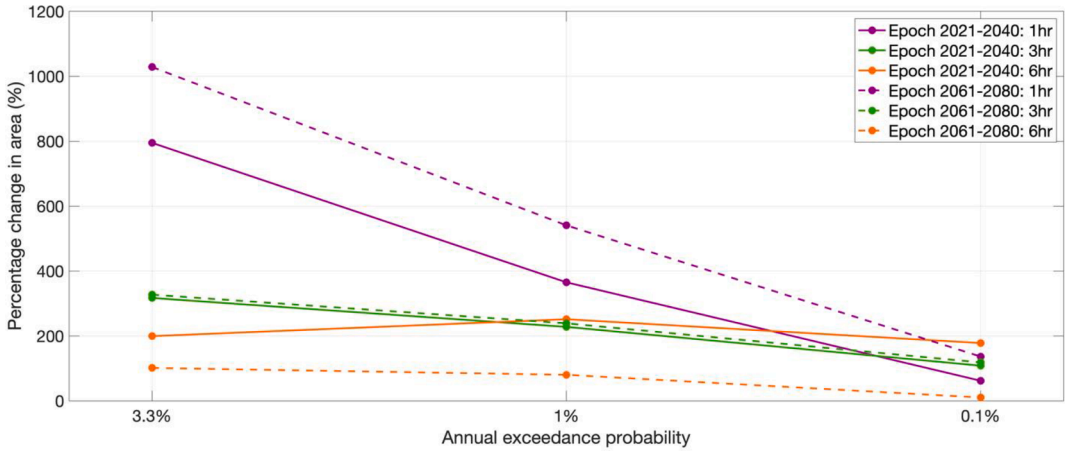

Fig. 11. Percentage change in total area flooded for Epochs 2021–2040 and 2061–2080 compared with the current climate conditions.

for the 1-hour duration events (A, D, G), suggesting that even though the area being flooded rises (Fig. 11) as the total rainfall increases (Fig. 9) the water depth of the extra inundated areas is predominantly between 0 and 1 m. For the 3-hour and 6-hour duration events, however, the mean water depth increases over time, except for the 6-hour duration events in epoch 2061–2080 (which have smaller projected rainfall than those for 3-hour storms in the same epoch). This result suggests that as the duration of the rainfall events increases, the water depth of the extra inundated areas also increases to predominantly larger than 1 m. Areas of regions where water depth falls in ranges of [0 1], [1 2], [2 3], [3 4], [4 5] and [5 6] are provided in Table S9 for each of the scenarios.

Fig. 13 shows the probability density functions of velocity for all the scenarios. Numbers in the plots are the corresponding means and standard deviations (in brackets) of velocity. Similar to the trend for water depth, overtime (from baseline to epoch 2061–2080), the mean velocity decreases for the 1-hour duration events (A, D, G), suggesting that the velocity of the extra inundated areas is predominantly between 0 and 1 m/s. For the 3-hour and 6-hour duration events, however, the mean velocity increases over time, except for the 6-hour duration events in epoch 2061–2080 (which have smaller projected rainfall than those for 3-hour storms in the same epoch). This result suggests that as the duration of the rainfall events increases, the velocity of the extra inundated areas also increases to predominantly larger than 1 m/s. Areas of regions where water velocity falls in ranges of [0 1], [1 2], [2 3] and [3 4] are provided in Table S10 for each of the scenarios.

5.5. *Erosion and deposition depths*

Fig. 14 shows the erosion/deposition depth for the worst-case scenario – a 6-hour storm with an annual exceedance probability of 0.1% during epoch 2021–2040. Results for the other scenarios are displayed in the Supplementary Material (Figs. S11–13) and on the web-based DST. Erosion at the three locations mentioned above in Section 5.1 (riverbank at the Castle, Bitterbeck car park and east of Gote Road), is again observed in this case. Remarkable erosion and deposition (depths up to 4–5 m) also occur in and along the River Cocker. Five bridges over the Cocker connect the east and west parts of the town, and are under high risk of being damaged. The agricultural fields in the upstream and downstream areas of the River Derwent, and Fitz Park also experience significant erosion and deposition (depths up to 2 m). Erosion and deposition in the urban areas, such as the town centre, residential areas and roads, on the

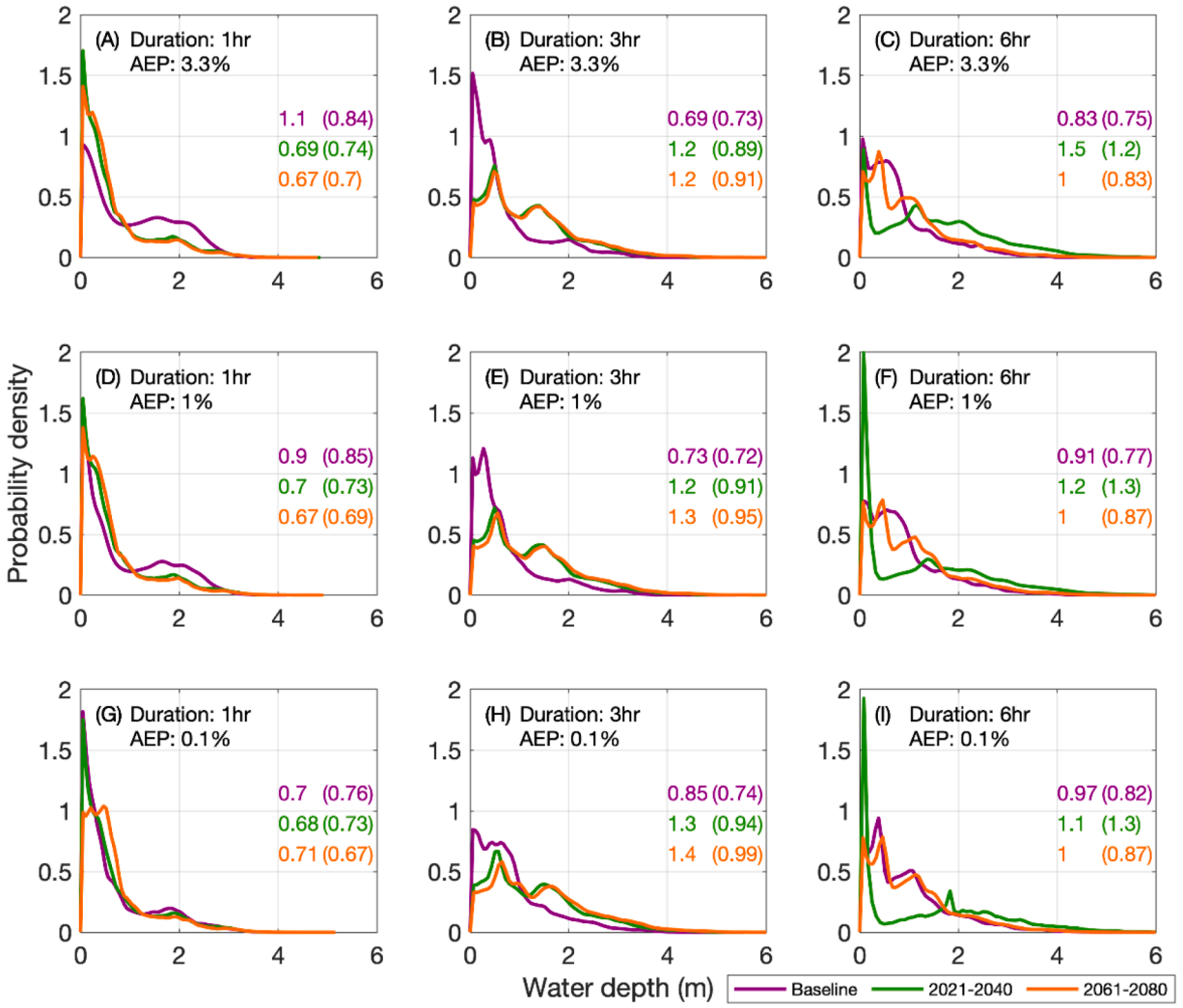

Fig. 12. Probability density functions of water depth for all the scenarios. From left to right, duration of events increases from 1 hour to 6 hours, and from top to the bottom, annual exceedance probability (AEP) decreases from 3.3% to 0.1%. Values of mean and standard deviation (in brackets) of water depth of the scenarios are provided in the figure, with colours of the numbers corresponding to the colours of the solid lines.

other hand, is less prominent.

Fig. 15 shows the probability density functions of erosion and deposition depth (E/D depth) based on cell counts. A large peak at ~0 m is observed for all the scenarios, and the majority of changes fall between −2 and 2 m. The distributions become taller as the duration increases, indicating an increase in E/D depth within the range of −0.5 to 0.5 m. The distribution also becomes wider through time, suggesting an increase in larger elevation changes (>0.5 m). In particular, a second peak at ~1 m is observed in most cases. The mean elevation changes in Fig. 16 show that there is small net deposition in all scenarios. This net deposition decreases with the duration of the events, but the variation with annual exceedance probability and climatic conditions, on the other hand, is small.

Areas of regions that undergo slight ([−0.15 0] & [0 0.15] m), significant ([−0.3–0.15] & [0.15 0.3] m) and extreme ([−∞ −0.3] & [0.3 +∞] m) elevation change are provided in Table S11. The areas of almost all the categories increase through time from the current climate conditions to epoch 2061–2080. The areas also increase as the duration of the rainfall event increases, except for the 6-hour duration events in epoch 2061–2080 which has less total rainfall than the 3-hour duration events in the same epoch. Viewed from a percentage perspective, the largest changes in area compared to the baseline are mostly for regions that undergo slight elevation changes. These results indicate that as the total rainfall increases, because of prolonged rainfall and climate change, the area susceptible to elevation change increases. A large portion of the extra area susceptible to elevation change, however, only experience slight erosion/deposition. On the other hand, Figs. S11–13 in the Supplementary material show that, without intervention, regions that undergo elevation changes under the current climate conditions are likely to experience a higher level of erosion and deposition as a result of climate change.

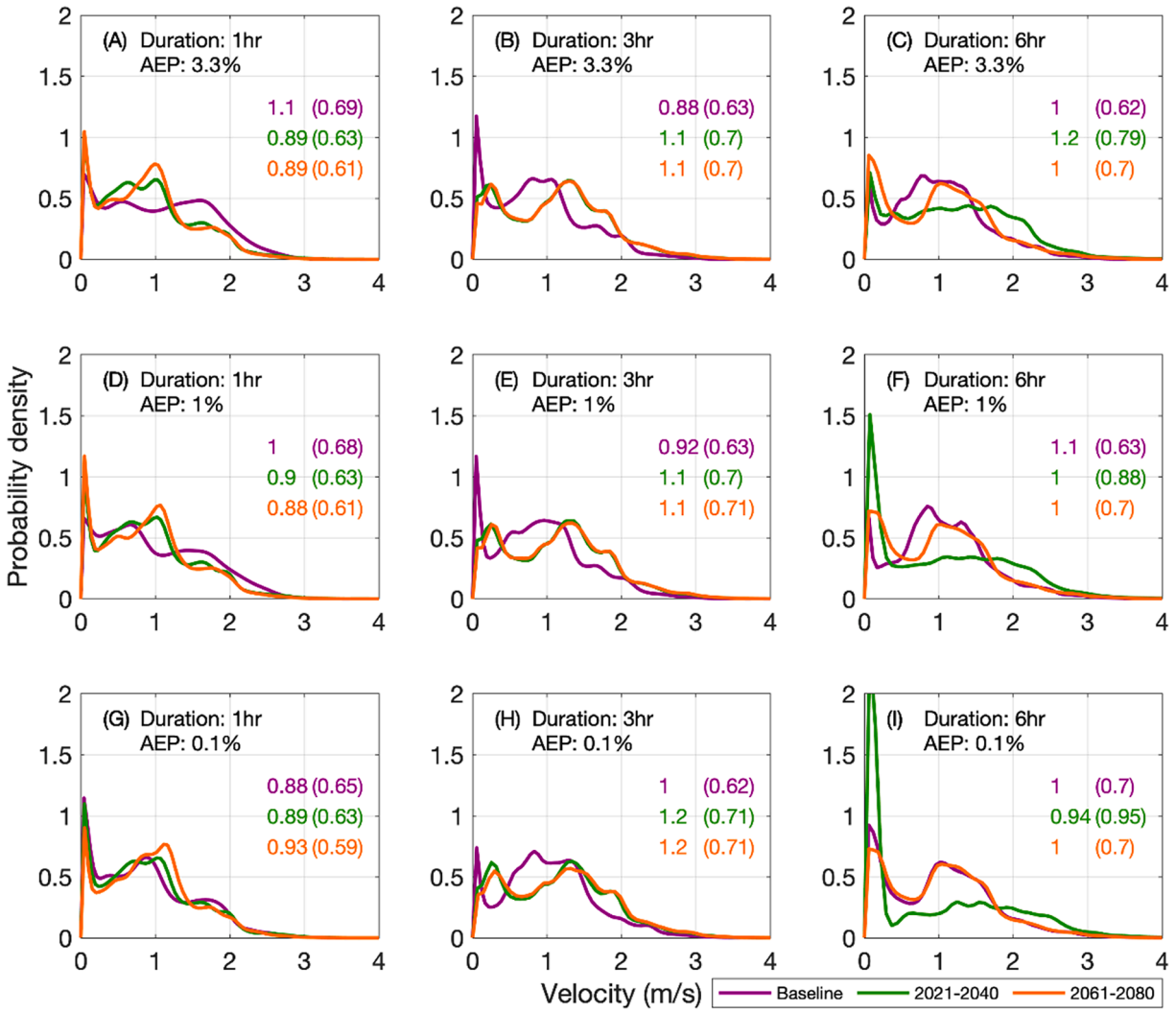

Fig. 13. Probability density functions of water velocity for all the scenarios. From left to right, duration of events increases from 1 hour to 6 hours, and from top to the bottom, annual exceedance probability (AEP) decreases from 3.3 % to 0.1 %. Values of mean and standard deviation (in brackets) of velocity of the scenarios are provided in the figure, with colours of the numbers corresponding to the colours of the solid lines.

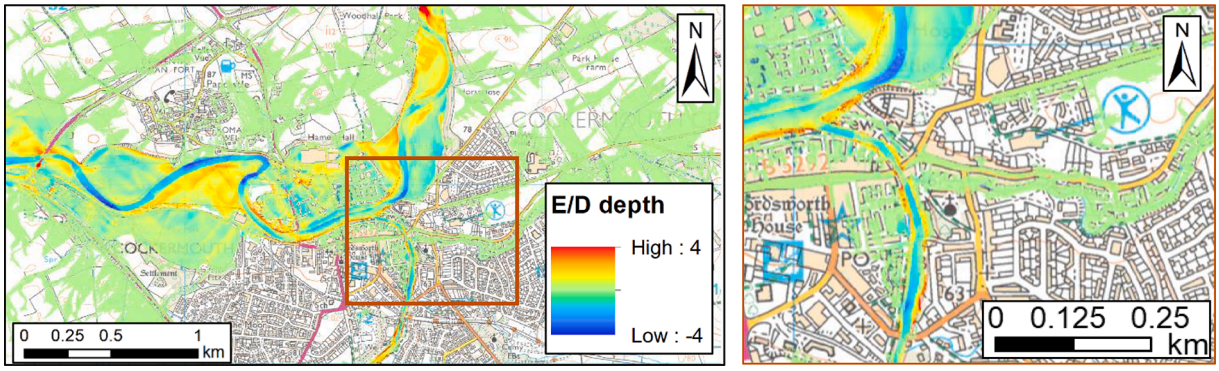

Fig. 14. Erosion/deposition depths (m) for the worst case scenario – a 6-hour storm with an annual exceedance probability of 0.1% during epoch 2021–2040. The scale shows changes in elevation (positive values indicate deposition; negative values indicate erosion).

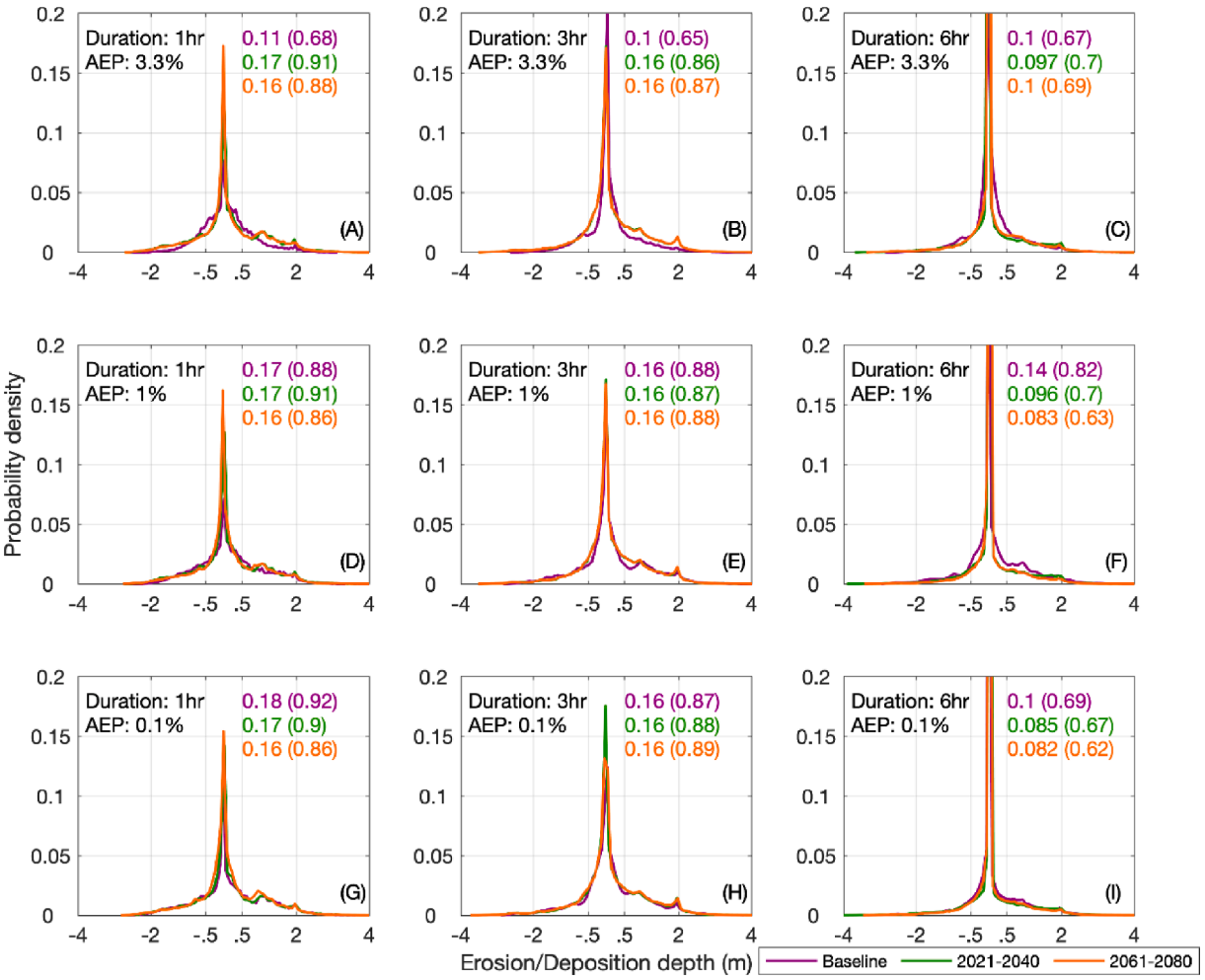

Fig. 15. Probability distributions of erosion (negative values) and deposition (positive values) depth (E/D depth). From left to right, duration of events increases from 1 hour to 6 hours, and from top to the bottom, annual exceedance probability (AEP) decreases from 3.3% to 0.1%. Values of mean and standard deviation (in brackets) are provided in the figure, with colours of the numbers corresponding to the colours of the solid lines.

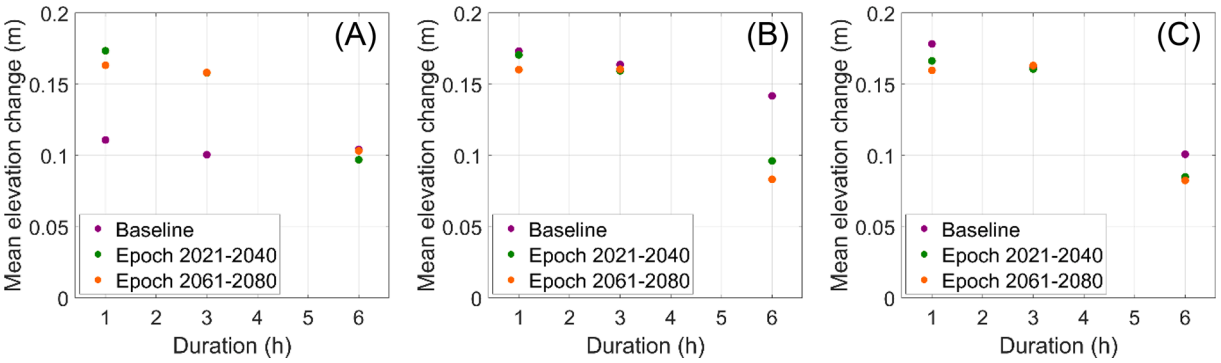

Fig. 16. Mean elevation change caused by storm events with annual exceedance probabilities of (A) 3.3%; (B) 1% and (C) 0.1%. Positive elevation change indicates deposition.

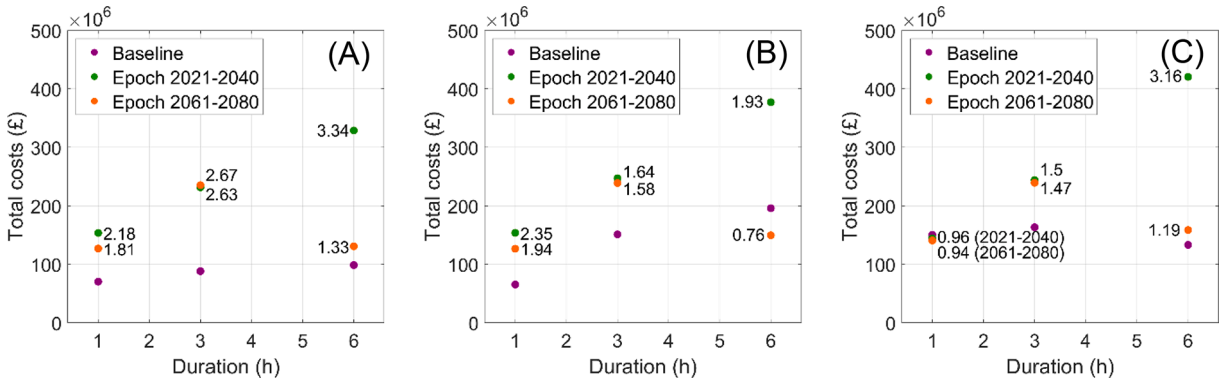

Fig. 17. Total costs of erosion and deposition for the three annual exceedance probabilities: (A) 3.3%; (B) 1%; and (C) 0.1%. Numbers in (B) and (C) are ratios between total cost of each future epoch and the current climate conditions (Baseline).

5.6. Economic loss from erosion and deposition

Fig. 17 shows the total costs of erosion and deposition damage for the scenarios of the three epochs. Costs associated with individual land use types, and their proportions of the total costs, are displayed in Table S12 and Fig. S14–16 in the Supplementary Material. The total costs show a similar trend to the rainfall totals in the DDF curves (Fig. 8). In other words, compared with the baseline, total costs for the two future epochs increase. For the current climate conditions (Baseline) and epoch 2021–2040, total costs increase as storm duration becomes longer (by as much as £277 M). For epoch 2061–2080, however, as a result of lower rainfall totals, the total costs for the 6-hour duration events are £81 M to £104 M less than those for the 3-hour duration events. The percentage increase in total cost compared with the baseline also increases with duration except for 6-hour storms in epoch 2061–2080.

For 26 (out of 27) scenarios, costs associated with damages caused to bridges contribute the largest proportions of the total costs (Table S12). The average cost associated with bridge damage is £114 M, and the average proportion of the total cost associated with bridges is 60.0%. The second highest costs are associated with sediment deposition in the urban fabric; the average cost is £43 M, with an average proportion of 22.6%. The rest of the average costs in a descending order are costs associated with land (£22 M, 11.6%), buildings (£8M, 4.2%) and roads (£3M, 1.6%). Even though the costs associated with buildings and roads are relatively small, the relative increase in cost as a result of a climate shift in the two future epochs is large: 50.7/11.3 and 9.7/7.3 fold increases, respectively. The costs associated with sediment deposition in the urban fabric also experience relatively large increases: 9.1 and 4.0 fold for the two epochs, respectively. Relative increases in the costs associated with bridges and agricultural land, on the other hand, are small: 1.6/1.3 and 1.9/1.7, respectively.

Trends with duration and annual exceedance probability can also be derived from Table S12. For instance, for the current climate conditions and for annual exceedance probability of 3.3%, costs associated with bridges increase by 25% from a 1-hour to a 6-hour storm. On the other hand, for the current climate conditions and for the 1-hour storms, costs associated with bridges increase by 122% from the highest to the lowest exceedance probability. The increase from 1-hour to 6-hour storm is much higher for buildings and roads at 1500% and 1660%. The increase from the highest to the lowest exceedance probability for buildings and roads, however, is more comparable to that associated with bridges, at 150% and 190%.

EAD values for each land-use type and each epoch are presented in Table S12. EAD values show similar trends to the averaged costs for each epoch. Bridges have the largest EADs (£4M to £6M), followed by the urban fabric (£1M to £4M). The EADs of bridges are within the same order of magnitude of the costs (£15.77 M according to Affleck & Gibbon, 2016) incurred to replace the Northside road bridge at Workington which collapsed during the November 2009 flood. Buildings and roads, again, have the relatively lowest EADs under the current climate conditions, but experience larger increases as the climate shifts (between a 9.2 and 14.9 fold increase for roads and between a 69 and 245.5 fold increase for buildings). From the current climate conditions to epoch 2021–2040, both the EAD and average cost increase for all land use types. EADs and average costs for epoch 2061–2080, however, are less than those for epoch 2021–2040. These reduced costs occur because the 6-hour duration events in epoch 2061–2080 produce less rainfall than those in epoch 2021–2040 and, therefore, cause less erosion and deposition.

6. Discussion

The novelty of the modelling framework lies in the following three aspects: 1) hourly rainfall data from the recently released climate projections (UKCP18) is used to create DDF curves and corresponding hydrographs and hyetographs for the coming two epochs to drive a hydro-sedimentary numerical model; 2) a hybrid approach, which combines the strength of the reach mode and the catchment mode of the model CAESAR-Lisflood, is adopted so that erosion hazards in the both the hillslope and fluvial system are assessed; and 3) economic loss resulting from erosion damage is quantified for different land-use types based on new non-linear depth-cost curves.

6.1. The effect of climate change on rainfall, flooding and erosion hazards

The DDF curves, showed that, because of a warming climate, rainfall totals for the two future epochs are likely to increase in the Cockermouth area. They also revealed that, for the current climate conditions and epoch 2021–2040, rainfall totals increase with storm duration. However, for epoch 2061–2080, rainfall totals for 6-hour storms were smaller than those for 3-hour storms, indicating the climate is likely to move towards shorter duration events with higher rainfall and longer duration events with less rainfall.

Located in the higher mid-latitudes and on the west coast of the Eurasia continent, the UK's climate is the marine west-coast type, which is characterised by moderate temperatures year-round and the absence of a dry season. Western sea breezes ease temperatures and cause cloudy weather to predominate, leading to regular precipitation, but with a distinct maximum in winter and a distinct minimum in summer. Geographically close to the UK is the Mediterranean region after which the Mediterranean climate type is named. Similar to the marine west coast climate type, the Mediterranean climate type represents dry summers and moist winters, but with stronger seasonal variability in precipitation and higher temperatures (Strahler, 2008). Rainfall events of the Mediterranean climate type are also sporadic with shorter duration events carrying larger amounts of rainfall, whereby catastrophic flash floods frequently occur (Altinbilek et al., 1997; Rebora et al., 2013). With global warming, the temperatures in the UK are rising (Tinker et al., 2020) and the changes in storm regimes presented in this paper suggest that the climate in Cockermouth, and more broadly in the UK, is seemingly shifting towards the Mediterranean climate type. Unlike the Mediterranean climate type, in which the dry summers are caused by high pressure from the Hadley cell, the projected drier summers in the UK are found to be associated with projected higher mean surface pressure across the British Isles for the summer months (Haarsma et al., 2015). Given erosion and deposition are driven by runoff hydraulics, maps of erosion and deposition (Fig. S9–12) closely follow those of flood extent, depth and velocity: under the current climate conditions, the areas that undergo erosion and deposition are confined to the river channels and open spaces such as fields and parks. As the climate shifts, the areas affected by erosion and deposition expand extensively to urban areas, even for short duration events with high probabilities of occurrence. This change occurs because the total area flooded was positively related to rainfall total. Of particular interest is that as the climate shifts towards shorter duration events with higher rainfall in epoch 2061–2080, the total area being flooded for the 6-hour duration storms was smaller than those for the 3-hour duration events. Intuitively, viewed from a perspective of percentage change, through time the warming climate is likely to lead to more significant rises in total inundation and erosion/deposition areas for short duration events with higher annual exceedance probability.

The water depth, water velocity and E/D depth of the extra flooded areas (compared with those of the current climate conditions), span large ranges of 0–6 m, 0–4 m/s and −4–4 m, respectively. Therefore, the large ranges were broken down to smaller intervals, and the areas of each interval were calculated to fully understand the significance of the extra flooded area in relation to erosion hazards. Changes in probability density functions of water depth and velocity (Fig. 13 and 14), as well as the spreading of the total area across the intervals (Tables S9–10), indicated that for the 1-hour duration events, the water depth and velocity of the extra inundated areas was predominantly 0–1 m and 0–1 m/s. However, as the duration increased, the water depth and velocity of the extra inundated areas increased to predominantly 1–2 m and 1–2 m/s. Exceptions are the 6-hour duration events in epoch 2061–2080 which, with lower rainfall totals, witnessed predominantly 0–1 m water depth and 0–1 m/s water velocity in the extra inundated areas. Similarly, with climate change, areas that experienced erosion and deposition increased significantly, but elevation changes in these extra areas was mostly between −0.3 to 0.3 m, i.e. between slight and significant elevation changes. The E/D depth of the areas that experience erosion and deposition in current climatic conditions, however, are likely to be exacerbated by climate change. In summary, in all but one scenario (2061–2080, 6-hour storms) the results suggest that climatic shifts may increase the areas of Cockermouth that undergo flooding, erosion and deposition, as well as increase the magnitude of the hazard.

The economic damage caused by erosion and deposition was also positively related to rainfall total. Therefore, economic costs increased with storm duration, and increased as the annual exceedance probability decreased. With the storm regimes shifting towards shorter duration events with higher intensity, the costs of 3-hour duration events were higher than those of 6-hour duration events in epoch 2061–2080. The highest costs are likely to be associated with damage caused to bridges, followed by urban sediment deposition, agricultural land, buildings and roads. A comparison was sought between these predicted economic costs and those of recent storm events in Cockermouth, particularly the November 2009 and 2015 storm Desmond floods, to gain some indication of the validity of these predictions. Unfortunately, costs are only available for the county of Cumbria as a whole, and include both direct and indirect costs (Cumbria County Council, 2011; Association of British Insurers, 2016). For example, in calculating the cost to buildings, financial reports not only include the direct cost of physical damage but also the indirect costs such as replacing damaged items, cleaning up, temporary alternative accommodation and loss of income from commercial buildings. Furthermore, the reported costs are for all flood-related impacts but the modelling framework only considers the costs associated with erosion and deposition. Thus, not only would the reported total costs differ significantly from our estimate but also, most likely, the proportion of total costs for each asset type because the asset profile of Cockermouth differs strongly to other areas in Cumbria. For example, Cockermouth has five road bridges confined within a small area surrounding a confluence of two rivers, and thus bridge damage formed a high proportion of the total costs. Such a high proportion would not be reflected so highly elsewhere in Cumbria.

6.2. Uncertainties in the modelled results

The results should be considered in light of key sources of uncertainty within the model chain, such as climate change scenario selection, model parameter specification, model input generation and the calculation of economic costs.

The selection of the two epochs and emission scenarios was dictated by the availability of the climate projection data and the choice of the three annual exceedance probabilities was to ensure the simulations represented consequences of temperate to severe storm

events, as used in UK flood risk predictions (Environment Agency, 2013). Choosing a single representative critical storm duration to represent catchment response is difficult because this duration is strongly related to the topography of the catchment, and any modelled area includes a number of sub-catchments of different shape, steepness and size (Environment Agency, 2013). For example, on hillslopes the critical duration is typically short because the greatest runoff is generated by high intensity rainfall, whereas in flatter areas, such as on floodplains, the critical duration is longer because surface runoff drains into these areas from over a much larger area. Thus, three storm durations were explored. Despite being designed to include a range of storm scenarios, the modelling framework was not applied to an ensemble of climate projections - an approach that takes variability into consideration and hence increase the reliability of long-term projections (Murphy et al., 2004; Li et al., 2019). The results presented in this work, therefore, could reflect the impact of both long-term climate regime shift as well as inherent variability.

The hydro-sedimentary model, CAESAR-Lisflood inevitably contains a number of parameters which require user input. Some of these parameters are to ensure the calculated results are within a reasonable range and the model is stable, such as the Courant number in the flow routing sub-model and the maximum allowable elevation change in the sediment transport sub-model. The more important ones, however, are those that have physical meaning, such as the hydraulic conductivity parameter *m*, and the suspended sediment settling velocity. The assigning of values to these parameters, according to the environment and scenarios being modelled, are discussed in detail in Meadows (2014) and Feeney et al. (2020). Due to the lack of validation data and the short storm durations considered, lateral migration of the river channel was not activated and most of the model parameters were set to their default values (see Table S7 for details). The hydraulic conductivity parameter *m*, on the other hand, was calibrated to create runoff with high resemblance to those observed in the River Derwent during storm Desmond, and was set to be uniform across the model domain. The values of these parameters were carried over into the future scenario simulations, even though the catchment characteristics may undergo changes over time. This approach was taken to reduce the complexity of the model inputs and to increase the comparability between model results of different epochs. Nonetheless, when interpreting the results presented herein, one should keep these constraints of the model in mind and focus more on the relative changes and the directions of change, instead of the absolute values.

Model uncertainties also arise from the choice and generation of model inputs. For example, even though the model domain is within an area of highly nonuniform topography, where the rainfall could vary spatially due to orographic effects, the rainfall in the catchment mode was assumed to be uniform. Given this uniform rainfall is generated based on annual maxima within the area, the input rainfall could be overestimated. Further, the depth-cost curves for damage calculations could be another source of uncertainty, and incorporating more empirical data into their construction could improve their reliability.

6.3. Implications for managing erosion hazards

The new erosion hazard modelling framework can help support operational (immediate) and strategic (medium to long term i.e. 10 + years) erosion control decision making through the provision of an assessment of the scale and consequences of erosion. First, the erosion and deposition maps can be used to identify areas and infrastructure (by asset type) presently at risk (likelihood and extent) and vulnerable (economic loss) to erosion events. Within Cockermouth, the results for example reveal that bridges and the castle on the riverbank of the River Derwent have the highest vulnerability. Second the results show the extent to which this erosion risk changes with climate, highlighting the differential vulnerability of particular assets. For instance, the maps show that for the current climate conditions, erosion and deposition is mainly restricted to the river channels and open spaces such as agricultural fields and parks. However, in the future two epochs, erosion and deposition is also predicted in residential and commercial areas for events with shorter durations (durations of 3 and 6 hours) and lower annual exceedance probabilities of 1% and 0.1%, causing substantial potential damage to roads and sediment deposition in the urban fabric. Third, the EAD estimates give an indication of where and when investment resources should be deployed. Specifically, the difference in EAD estimates between current and future climate conditions represent the costs that can be averted if appropriate interventions are put in place. Thus, they show which assets are vulnerable and

Table 2
Costs associated with bridge damage in Cumbria caused by the 2009 and 2015 floods.

Bridge	Cost (£)	Description
Pooley Bridge	5 M (Stein, 2020)	A stainless steel road bridge was built over the River Eamont to replace the 18th Century stone structure destroyed during storm Desmond in December 2015.
Old Gowan Bridge	0.5 M (BBC, 2017)	The Old Gowan Bridge, which links the village of Staveley, near Kendal, with the A591, was damaged beyond repair in the December 2015 floods.
Brougham Old Bridge	0.75 M (Cumbria Crack, 2017)	The 200-year old English Heritage listed bridge was devastated during storm Desmond and was later repaired and reinforced.
Middleton Bridge	0.55 M (Cumbria County Council, 2019)	A new bridge was built to replace the severely damaged Middleton Hall Bridge on the A683 during storm Desmond.
Victoria Bridge	0.74 M (Dicicco, 2019)	Severely damaged during storm Desmond in 2015 and required repairs.
Bell Bridge	1.1 M (ITV Border, 2017)	A new bridge was built to replace the original structure which was damaged during storm Desmond and other storms, leading to its collapse during Storm Jonas in 2016.
Millers Bridge in Cockermouth	150,000 (Cumbria County Council, 2009)	Suffered severe damage in the 2009 floods, with a section of the structure collapsing into the River Derwent. Part of the bridge had to be rebuilt and extended to fit the new shape of the river banks, which were heavily eroded by the flood water.
Navvies Bridge in Workington	1.7 M (Affleck & Gibbon, 2016)	Washed away in the 2009 floods and rebuilt for pedestrians and cyclists.

require investment now to ensure they stay resilient to extreme storm events in the future and which are likely to be vulnerable and require investment in the future. In Cockermouth, these estimates clearly show that bridges require investment now to avoid failure, such as the destruction of the Northside road bridge at Workington during the November 2009 flood, which caused a fatality and cost £15.77 M (£4.6 M for a temporary bridge and £11.17 M for a new permanent bridge) to replace (Affleck & Gibbon, 2016). Table 2 further lists costs associated with other bridge damage in Cumbria caused by recent storm events. Storm Desmond alone damaged a total of 557 bridges, including three being washed away, costing £117 M. Damage to critical infrastructure, such as bridges and roads, can also cause considerable transport disruptions, leading to exacerbated storm-induced economic costs and lowered community welfare (Cumbria County Council, 2010). For example, 25 bridge closures in Cumbria due to the 2009 floods caused increased travel time costing the private and public sectors an estimated £2M per week during a six-month diversion (Affleck & Gibbon, 2015). The modelling framework can highlight where precautionary measures are required to increase the resilience of bridges, being highly beneficial in both financial and societal terms. Intervention may also likely be needed within the next 20 years to avert the economic costs associated with significant sediment deposition in the urban fabric and erosion damage to roads and agricultural land.

The focus of this paper has been on showcasing the broad feasibility of the modelling framework for a range of asset types in one study area. Clearly future work needs to investigate further the impacts of climate change on erosion hazards in different river catchments, particularly those with contrasting meteorological and catchment properties, such as topography, soils, steepness and size. Further, the vulnerability of other asset types needs to be assessed, such as electricity supply networks (e.g. an electricity sub-station along the River Severn was forced to close during the UK summer 2007 floods), flood defences, and dams. In addition further work could focus on using the economic damage estimates to aid stakeholders in making decisions about erosion control intervention. For example, the EAD estimates, combined with estimates of the full economic costs of erosion control, would allow a real options approach to be used to estimate Net Present Value, as applied for the control of coastal flooding (Prime et al., 2018). This approach uses the uncertainty surrounding the storm event projections to determine if investment in erosion control is required now or if there is value in deferring the investment for a defined period. In addition, risk could be considered in terms of economic damage per year for the various scenarios to produce cost-benefit assessments to calculate the most efficient investment options. Such an approach may also be used to help decide the best time to deploy these options and where, for example, which sections of riverbanks require erosion control, or which bridges would benefit most from resilience measures. Further the modelling framework could be expanded to examine indirect economic costs, such as those on ecosystem services (e.g. water and habitat quality), water treatment and the exacerbation of flooding due to river channel erosion and deposition. In addition, the influence of sequences of storm events - and the impact of climate change on this sequencing - on erosion hazards needs to be considered. For example, a previous storm may make areas of the catchment more or less vulnerable to future storms, dependent upon factors such as storm duration and intensity, sediment availability and catchment topography.

6.4. Applicability of the model framework

In summary, the new modelling framework provides an integrated mechanism for visualising how future erosion risk compares with the present, and where and when erosion control may need to be implemented according to the type of asset and the scale of the problem. Thus, the modelling output provides stakeholders with an erosion hazard assessment that can ultimately feed into a strategy that builds climate change resilience. Although the focus in this paper has been on one upland case study, this framework can be applied to other catchment systems in the UK. For lowland catchments, the highly topography-dependent flow routing algorithm in CAESAR-Lisflood may lead to flow stagnation, and thus model parameters must be assigned carefully. On the other hand, the multiple flow direction algorithm is suitable for simulating different river systems, including braided rivers on alluvial fans, river deltas, and across depositional plains (Coulthard et al., 2002). In theory, with modifications to the derivation of the national-specific hyetographs and hydrographs, the modelling framework could be extended to other systems globally. However, in practice, the application of the modelling framework requires high resolution terrain and land use data which may not be available in some regions of the world. Further, parameterisations of the erosion processes represented in the model may differ in other environments, particularly semi-arid and tropical environments, due to their distinctive biomes. Therefore, when applying this modelling framework to other environments, modifications are likely needed to the hydro-sedimentary model component to faithfully replicate the topographically-driven hydraulic and erosional processes.

7. Conclusion

A novel erosion-hazard modelling framework has quantified, for the first time, how the risks posed by erosion hazards, and their economic impacts on critical infrastructure, may change in a warming UK climate. Using a UK upland catchment as a case study, the results revealed: 1) owing to a warming climate, total rainfall in the Cockermouth area (and likely across the UK) may be higher for all storm durations and annual exceedance probabilities, until epoch 2061–2080 when the rainfall regime is likely to shift towards shorter duration events with higher rainfall and longer duration events with less rainfall; 2) the total area that undergoes flooding, erosion and sediment deposition is positively related to rainfall total, and thus this area, as well as the magnitude of the hazard, may increase with climate change; 3) the economic damage caused by erosion and deposition is also positively related to rainfall total, and the highest costs are likely to be associated with damage caused to bridges, followed by sediment deposition in the urban fabric, and erosion damage to agricultural land, buildings and roads; and 4) according to the EAD estimates, bridges in the Cockermouth area require investment now to ensure their resilience to extreme storm events, and interventions are needed within the next 20 years to prevent high economic costs associated with significant sddiment deposition in the urban fabric and erosion damage to roads and agricultural

land.

The paper reveals that this integrated erosion-hazard modelling framework can support operational (immediate) and strategic (medium to long term i.e. 10+ years) erosion control decision making, through the provision of an assessment of the scale and consequences of erosion. The framework provides a new tool for visualising how future erosion risk compares with the present, and where and when erosion control may need to be implemented according to the type of asset and the scale of the problem.

Declaration of Competing Interest

The authors declare that they have no known competing financial interests or personal relationships that could have appeared to influence the work reported in this paper.

Acknowledgments

This work was supported by the UK Natural Environment Research Council research grant: 'Erosion Hazards in River Catchments: Making Critical Infrastructure More Climate Resilient' (NE/S01697X/1). The authors would like to thank Philip Knight (Natural Resources Wales) for the development of the Decision Support Tool and Christopher Feeney (UK Centre for Ecology and Hydrology) for his advice on the use of CAESAR-Lisflood.

Appendix A. Supplementary data

Supplementary data to this article can be found online at https://doi.org/10.1016/j.crm.2021.100287.

References

Affleck, A., Gibbon, J., 2015. Valuing the social benefits of local infrastructure in Workington, iBUILD briefing paper 9. [online] Available at: https://research.ncl.ac.uk/media/sites/researchwebsites/ibuild/WP9.pdf [Accessed 10 December 2020].

Affleck, A., Gibbon, J., 2016. Workington: A case study in coordination and communication. In Proceedings of the Institution of Civil Engineers-Municipal Engineer, 169(2), 109-117. Thomas Telford. London.

Altinbilek, D., Barret, E.C., Oweis, T., Salameh, E., Siccardi, F., 1997. Rainfall Climatology on the Mediterranean, EU-AVI 080 Project ACROSS—Analyzed climatology rainfall obtained from satellite and surface data in the Mediterranean basin. EC Rep. EC reports.

Araújo, M.B., Rahbek, C., 2006. How does climate change affect biodiversity? Science 313 (5792), 1396–1397.

Association of British Insurers, 2016. New figures reveal scale of insurance response after recent floods. [online] Available at: https://www.abi.org.uk/news/news-articles/2016/01/new-figures-reveal-scale-of-insurance-response-after-recent-floods/. [Accessed 10 December 2020].

Bates, P.D., Horritt, M.S., Fewtrell, T.J., 2010. A simple inertial formulation of the shallow water equations for efficient two-dimensional flood inundation modelling. J. Hydrol. 387 (1–2), 33–45.

BBC, 2017. Replacement for flood-damaged bridge in Staveley opens. [online] Available at: https://www.bbc.co.uk/news/uk-england-cumbria-39968127 [Accessed 10 December 2020].

Beven, K.J., 2011. Rainfall-runoff Modelling: The Primer. John Wiley & Sons, Chichester.

Beven, K.J., Kirkby, M.J., 1979. A physically based, variable contributing area model of basin hydrology/Un modèle à base physique de zone d'appel variable de l'hydrologie du bassin versant. Hydrol. Sci. J. 24 (1), 43–69.

Boardman, J., Evans, R., Favis-Mortlock, D.T., Harris, T.M., 1990. Climate change and soil erosion on agricultural land in England and Wales. Land Degrad. Dev. 2 (2), 95–106.

Chatterton, J., Viavattene, C., Morris, J., Penning-Rowsell, E.C., Tapsell, S.M., 2010. The Costs of the Summer 2007 Floods in England. Environment Agency, Bristol, UK.

Chow, V.T., 1959. Open-Channel Hydraulics. McGraw-Hill Book Company, New York.

Coles, D., Yu, D., Wilby, R.L., Green, D., Herring, Z., 2017. Beyond 'flood hotspots': modelling emergency service accessibility during flooding in York, UK. J. Hydrol. 546, 419–436.

Correa, S.W., Mello, C.R., Chou, S.C., Curi, N., Norton, L.D., 2016. Soil erosion risk associated with climate change at Mantaro River basin, Peruvian Andes. Catena 147, 110–124.

Costmodelling Limited, 2020. Typical UK construction costs of buildings. [online] Available at: https://costmodelling.com/building-costs [Accessed 07 December 2020].

Coulthard, T.J., Macklin, M.G., Kirkby, M.J., 2002. A cellular model of Holocene upland river basin and alluvial fan evolution. Earth Surf. Proc. Land. 27 (3), 269–288.

Coulthard, T.J., Neal, J.C., Bates, P.D., Ramirez, J., de Almeida, G.A., Hancock, G.R., 2013. Integrating the LISFLOOD-FP 2D hydrodynamic model with the CAESAR model: Implications for modelling landscape evolution. Earth Surf. Proc. Land. 38 (15), 1897–1906.

Coulthard, T.J., Skinner, C.J., 2016. The sensitivity of landscape evolution models to spatial and temporal rainfall resolution. Earth Surf. Dyn. 4 (3), 757.

Cumbria County Council, 2009. Cumbria Floods November 2009. [online] Available at: https://assets.publishing.service.gov.uk/government/uploads/system/uploads/attachment_data/file/61906/Transport-CumbriaFloods2009.pdf [Accessed 10 December 2020].

Cumbria County Council, 2010. Cumbria Floods November 2009: An impact assessment. [online] Available at: https://www.cumbria.gov.uk/eLibrary/Content/Internet/536/671/4674/4026717419.pdf [Accessed 10 December 2020].

Cumbria County Council, 2011. Cumbria floods November 2009 learning from experience recovery phase debrief report. [online] Available at: https://www.cumbria.gov.uk/eLibrary/Content/Internet/533/561/4066711109.pdf [Accessed 08 December 2020].

Cumbria County Council, 2019. Middleton Hall Bridge replacement set to open. [online] Available at: http://www.yourcumbria.org/News/2019/middletonhallbridgereplacementsettoopen.aspx [Accessed 08 December 2020].

Cumbria Cracker, 2017. Final stage of Brougham Old Bridge repair works to commence this week. [online] Available at: https://www.cumbriacrack.com/2017/07/31/final-stage-brougham-old-bridge-repair-works-commence-week/ [Accessed 10 December 2020].

de Castella, T., 2011. Should people build their own homes? [online]. Available at: https://www.bbc.co.uk/news/magazine-14125196 [Accessed 15 April 2020].

DEFRA, 2016. National Flood Resilience Review. Department for Environment, Food and Rural Affairs, London.

Deng, L., Wang, W., Yu, Y., 2016. State-of-the-art review on the causes and mechanisms of bridge collapse. Journal of Performance of Constructed Facilities, 30(2), 04015005.

Dicicco, L., 2019. Completion date for £740,000 project to fix Kendal's battered Victoria Bridge delayed until summer 2020. [online] Available at: https://www.in-cumbria.com/news/17896194.completion-date-740-000-project-fix-kendals-battered-victoria-bridge-delayed-summer-2020/ [Accessed 10 December 2020].
Dong, M., Hao, Y., Zhang, C., Li, L., 2017. Failure mechanism analysis of asphalt–aggregate systems subjected to direct shear loading. Mater. Struct. 50 (5), 218.
Environment Agency, 2013. What is the risk of flooding from surface water map? [online] Available at: https://assets.publishing.service.gov.uk/government/uploads/system/uploads/attachment_data/file/842485/What-is-the-Risk-of-Flooding-from-Surface-Water-Map.pdf [Accessed 08 December 2020].
Einstein, H.A., 1950. The bed-load function for sediment transportation in open channel flows. Technical Bulletin No. 1026, U.S. Dept. of Agriculture, Soil Conservation Service, Washington, D.C.
Favis-Mortlock, D., Boardman, J., 1995. Nonlinear responses of soil erosion to climate change: a modelling study on the UK South Downs. Catena 25 (1–4), 365–387.
Feeney, C.J., Chiverrell, R.C., Smith, H.G., Hooke, J.M., Cooper, J.R., 2020. Modelling the decadal dynamics of reach-scale river channel evolution and floodplain turnover in CAESAR-Lisflood. Earth Surf. Proc. Land. 45 (5), 1273–1291.
Fewtrell, T.J., Duncan, A., Sampson, C.C., Neal, J.C., Bates, P.D., 2011. Benchmarking urban flood models of varying complexity and scale using high resolution terrestrial LiDAR data. Physics and Chemistry of the Earth, Parts A/B/C 36 (7–8), 281–291.
Fluixá-Sanmartín, J., Altarejos-García, L., Morales-Torres, A., Escuder-Bueno, I., 2018. Climate change impacts on dam safety. Natural Hazards and Earth System Sciences, 18(9), 2471-2488.
Graves, A.R., Morris, J., Deeks, L.K., Rickson, R.J., Kibblewhite, M.G., Harris, J.A., Farewell T.S., Truckle, I., 2015. The total costs of soil degradation in England and Wales. Ecological Economics, 119, 399-413.
Guan, M., Carrivick, J.L., Wright, N.G., Sleigh, P.A., Staines, K.E., 2016. Quantifying the combined effects of multiple extreme floods on river channel geometry and on flood hazards. J. Hydrol. 538, 256–268.
Haarsma, R.J., Selten, F.M., Drijfhout, S.S., 2015. Decelerating Atlantic meridional overturning circulation main cause of future west European summer atmospheric circulation changes. Environ. Res. Lett. 10 (9).
Haregeweyn, N., Tsunekawa, A., Poesen, J., Tsubo, M., Meshesha, D.T., Fenta, A.A., Nyssen, J., Adgo, E., 2017. Comprehensive assessment of soil erosion risk for better land use planning in river basins: Case study of the Upper Blue Nile River. Sci. Total Environ. 574, 95–108.
Hertfordshire County Council, 2020. An introduction to highway maintenance. [online] Available at: https://www.hertfordshire.gov.uk/statweb/meetingsnov04toapr13/Highways%20Maintenance%20Topic%20Group/20110624/Appendix%20G.pdf [Accessed 07 December 2020].
Hoang, L., Fenner, R.A., 2016. System interactions of stormwater management using sustainable urban drainage systems and green infrastructure. Urban Water J. 13 (7), 739–758.
Home Advisor, 2019. How much does it cost to repair & cleanup water damage? [online] Available at: https://www.homeadvisor.com/cost/disaster-recovery/repair-water-damage/ [Accessed 15 April 2020].
Home Guide. (2019). How much does it cost to repair a foundation? [online] Available at: https://homeguide.com/costs/foundation-repair-cost [Accessed 15 April 2020].
Howard, A.J., Knight, D., Coulthard, T., Hudson-Edwards, K., Kossoff, D., Malone, S., 2016. Assessing riverine threats to heritage assets posed by future climate change through a geomorphological approach and predictive modelling in the Derwent Valley Mills WHS, UK. J. Cult. Heritage 19, 387–394.
Huang, W., Ho, H.C., Peng, Y., Li, L., 2016. Qualitative risk assessment of soil erosion for karst landforms in Chahe town, Southwest China: a hazard index approach. Catena 144, 184–193.
HR Wallingford, 2006. Flood risks to people Phase 2: The flood risks to people methodology. (FD2321/TR1). Department for Environment, Food and Rural Affairs, London.
ITV Border (2017). Historic bridge rebuilt in Cumbria after £1.1m project. [online] Available at: https://www.itv.com/news/border/2017-12-19/reopening-of-200-year-old-bridge-reconnects-flood-hit-communities-in-cumbria [Accessed 10 December 2020].
Kellogg, W.W., 2019. Climate change and society: Consequences of increasing atmospheric carbon dioxide. Routledge. New York.
Kjeldsen, T.R., Stewart, E.J., Packman, J.C., Folwell, S.S., Bayliss, A.C., 2005. Revitalisation of the FSR/FEH rainfall-runoff method. Final Report to DEFRA/EA, CEH, Wallingford. (FD1913/TR).
Koks, E.E., Rozenberg, J., Zorn, C., Tariverdi, M., Vousdoukas, M., Fraser, S.A., Hall, J.W., Hallegatte, S., 2019. A global multi-hazard risk analysis of road and railway infrastructure assets. Nat. Commun. 10 (1), 1–11.
Lane, S. N., Landström, C., Whatmore, S.J., 2011. Imagining flood futures: risk assessment and management in practice. Philos. Trans. Royal Soc. A: Math. Phys. Eng. Sc., 369(1942), 1784-1806.
Li, X., Leonardi, N., Plater, A.J., 2019. A stochastic approach to modelling tidal creek evolution: Exploring environmental influences on creek topologies through ensemble predictions. Geophys. Res. Lett. 46 (23), 13836–13844.
Li, Y., Gong, J., Niu, L., Sun, J., 2019. A physically based spatiotemporal method of analyzing flood impacts on urban road networks. Nat. Hazards 97 (1), 121–137.
Lowe, J.A., Bernie, D., Bett, P., Bricheno, L., Brown, S., Calvert, D., Clark, R., Eagle, K., Edwards, T., Fosser, G., Fung, F., 2018. UKCP18 science overview report. Met Office Hadley Centre: Exeter, UK.
Manning, R., 1890. On the flow of water in open channels and pipes. Trans. Inst. Civil Eng. Ireland, 20, 161–207.
Matthews, T., Murphy, C., McCarthy, G., Broderick, C., Wilby, R.L., 2018. Super Storm Desmond: a process-based assessment. Environ. Res. Lett. 13 (1).
McCall, I.; Evans, C. (2016) Cockermouth. S. 19 flood investigation report. Environment Agency, Cumbria County Council: Penrith, UK.
McGowan, P., 2016. Cost of floods revealed – and where Cumbria council spent money. [online] Available at: https://www.newsandstar.co.uk/news/16761567.cost-of-floods-revealed-and-where-cumbria-council-spent-money [Accessed 15 April 2020].
Meadows, T., 2014. Forecasting long-term sediment yield from the Upper North Fork Toutle River, Mount St Helens, USA. PhD thesis, University of Nottingham.
Merz, B., Kreibich, H., Schwarze, R., Thieken, A., 2010. Review article" Assessment of economic flood damage". Nat. Hazards Earth Syst. Sci. 10 (8), 1697.
Milly, P.C.D., Wetherald, R.T., Dunne, K.A., Delworth, T.L., 2002. Increasing risk of great floods in a changing climate. Nature 415 (6871), 514–517.
Mizuta, R., 2012. Intensification of extratropical cyclones associated with the polar jet change in the CMIP5 global warming projections. Geophys. Res. Lett. 39 (19), L19707. https://doi.org/10.1029/2012GL053032.
Murphy, J.M., Sexton, D.M., Barnett, D.N., Jones, G.S., Webb, M.J., Collins, M., Stainforth, D.A., 2004. Quantification of modelling uncertainties in a large ensemble of climate change simulations. Nature 430 (7001), 768–772.
My Job Quote, 2019. Average cost of unblocking and cleaning a drain. [online] Available at: https://www.myjobquote.co.uk/costs/clean-and-unclog-drains [Accessed 15 April 2020].
Morris, J., Brewin, P., 2014. The impact of seasonal flooding on agriculture: the spring 2012 floods in Somerset, England. J. Flood Risk Manage. 7 (2), 128–140.
Overeem, A., Buishand, A., Holleman, I., 2008. Rainfall depth-duration-frequency curves and their uncertainties. J. Hydrol. 348 (1–2), 124–134.
Penning-Rowsell, E., Priest, S., Parker, D., Morris, J., Tunstall, S., Viavattene, C., Chatterton, J., Owen, D., 2014. Flood and coastal erosion risk management: a manual for economic appraisal. Routledge. New York.
Palmer, T.N., Räisänen, J., 2002. Quantifying the risk of extreme seasonal precipitation events in a changing climate. Nature 415 (6871), 512–514.
Pierce, F.J., Lal, R., 2017. Monitoring the impact of soil erosion on crop productivity. In Soil erosion research methods (pp. 235-263). Soil Water Conservation Society (tandfonline.com).
Prime, T., Morrissey, K., Brown, J., Plater, A., 2018. Protecting energy infrastructure against the uncertainty of future climate change: a real options approach. Journal of Ocean and Coastal Economics, 5(1). https://doi.org/10.15351/2373-8456.1075.
Pritchard, O., Hallett, S.H., Farewell, T.S., 2013. Soil corrosivity in the UK – Impacts on critical infrastructure. ITRC–Infrastructure Transition Research Consortium, Cranfield University. Cranfield.
Rebora, N., Molini, L., Casella, E., Comellas, A., Fiori, E., Pignone, F., Siccardi, F., Silvestro, F., Tanelli, S., Parodi, A., 2013. Extreme rainfall in the Mediterranean: What can we learn from observations? J. Hydrometeorol. 14 (3), 906–922.

Rickson, J., Deeks, L., Posthumus, H., Quinton, J., 2010. To review the overall costs and benefits of soil erosion measures and to identify cost-effective mitigation measures. Sub-Project C of Defra Project SP1601: Soil Functions, Quality and Degradation–Studies in Support of the Implementation of Soil Policy. Department for Environment, Food and Rural Affairs, London.

Rothwell, J.J., Evans, M.G., Liddaman, L.C., Allott, T.E.H., 2007. The role of wildfire and gully erosion in particulate Pb export from contaminated peatland catchments in the southern Pennines, UK. Geomorphology 88 (3–4), 276–284.

Stein, J., 2020. Pooley Bridge - Single span steel structure replaces collapsed Victorian bridge. [online] Available at: https://www.newcivilengineer.com/innovative-thinking/pooley-bridge-single-span-steel-structure-replaces-collapsed-victorian-bridge-19-02-2020/#:~:text=The%20new%20%C2%A35M%20Pooley,it%20opens%20in%20this%20summer. [Accessed 10 December 2020].

Strahler, A.H., 2008. Modern Physical Geography. John Wiley & Sons, Chichester.

The Environment Agency, 2013. What is the risk of flooding from surface water map? (Report LIT 8988). Environment Agency, Bristol.

Thorne, C.R., Evans, E.P., Penning-Rowsell, E.C. (Eds.), 2007. Future Flooding and Coastal Erosion Risks. Thomas Telford. London.

Tinker, J., Howes, E., Wakelin, S., Menary, M., Kent, E., Berry, D. I., Hindson, J., Ribeiro, J., Dye, S., Andres, O., Lyons, K., 2020. The impacts of climate change on temperature (air and sea), relevant to the coastal and marine environment around the UK. MCCIP Science Review 2020 (pp. 1-30). Marine Climate Change Impacts Partnership. UK. doi: 10.14465/2020.arc01.tem.

Van De Wiel, M.J., Coulthard, T.J., Macklin, M.G., Lewin, J., 2007. Embedding reach-scale fluvial dynamics within the CAESAR cellular automaton landscape evolution model. Geomorphology 90 (3–4), 283–301.

Welsh, K.E., Dearing, J.A., Chiverrell, R.C., Coulthard, T.J., 2009. Testing a cellular modelling approach to simulating late-Holocene sediment and water transfer from catchment to lake in the French Alps since 1826. The Holocene 19 (5), 785–798.

Welter, G., Bieber, S., Bonnaffon, H., Deguida, N., Socher, M., 2010. Cross-sector emergency planning for water providers and healthcare facilities. J. American Water Works Assoc. 102 (1), 68–78.

Wilcock, P.R., Crowe, J.C., 2003. Surface-based transport model for mixed-size sediment. J. Hydraul. Eng. 129 (2), 120–128.

Yang, L., Scheffran, J., Qin, H., You, Q., 2015. Climate-related flood risks and urban responses in the Pearl River Delta, China. Regional Environ. Change 15 (2), 379–391.

Zappa, G., Shaffrey, L.C., Hodges, K.I., Sansom, P.G., Stephenson, D.B., 2013. A multimodel assessment of future projections of North Atlantic and European extratropical cyclones in the CMIP5 climate models. J. Clim. 26 (16), 5846–5862.